Figure 1   CD spectra of wIpTx_a and its analogues

The measurement was carried out in the UV range of 250–190 nm on a JASCO J-750 spectropolarimeter in solution (0.01 M sodium phosphate, pH 7.0) at 20 °C.

PEG, 1 mM EDTA and 50 mM Tris, pH 7.3) was added to each vial and was incubated for 5 min at room temperature (25 °C). Precipitated protein was sedimented for 5 min at 12000 g using an Eppendorf microcentrifuge, and the pellets were rinsed twice with 0.6 ml of the relevant ryanodine-binding buffer without radioactive ryanodine. The pellets were then solubilized in 100 μl of Soluene 350 (Packard) at 70 °C for 30 min, after which 4 ml of cocktail [Picofluor (Packard)] was added and the radioactivity was measured by liquid scintillation [32]. To minimize non-specific binding, 100-fold of non-radioactive ryanodine (Calbiochem) was included.

Statistical analysis

Results are given as means ± S.E.M. with the number of experiments. The S.E.M. is included within the Figure legends or indicated by error bars. Individual activation curves of RyR1 by wIpTx_a and analogues were fitted with the Hill equation using the Origin 4.1 software package (RockWare, Golden, CO, U.S.A.).

RESULTS AND DISCUSSION

Synthesis of wIpTx_a and analogues

Linear precursors of wIpTx_a and its alanine-scanning analogues were assembled by solid-phase methodology. The crude linear precursors were air-oxidized, and the properly folded products were purified by ion-exchange chromatography and reverse-phase HPLC (1–4% yield from the starting resin). CD spectra showed that secondary structures of all analogues, including L7A (Leu^7 → Ala), K22A (Lys^{22} → Ala), R23A (Arg^{23} → Ala), R24A (Arg^{24} → Ala), R31A (Arg^{31} → Ala) and R33A (Arg^{33} → Ala), were similar to that of wIpTx_a (Figure 1). Exceptionally, the linear analogue (Ala^{3,10,16,17,21,32})IpTx_a, which simultaneously replaced all six cysteine residues with alanine residues, showed a random conformation with a large negative Cotton effect (around 198 nm), indicating that the three intramolecular disulphide bonds in wIpTx_a play an important role in maintaining its overall structure.

Structure calculations of wIpTx_a

Complete proton assignments of all 33 amino acids in synthetic wIpTx_a were determined using traditional two-dimensional NMR sequential assignment techniques [33]. Identification of the amino acid spin system was based on scalar coupling patterns observed in DQF-COSY and HOHAHA experiments, complemented with the results of NOESY measurements. Figure 2 shows the NH-C$^\alpha$H
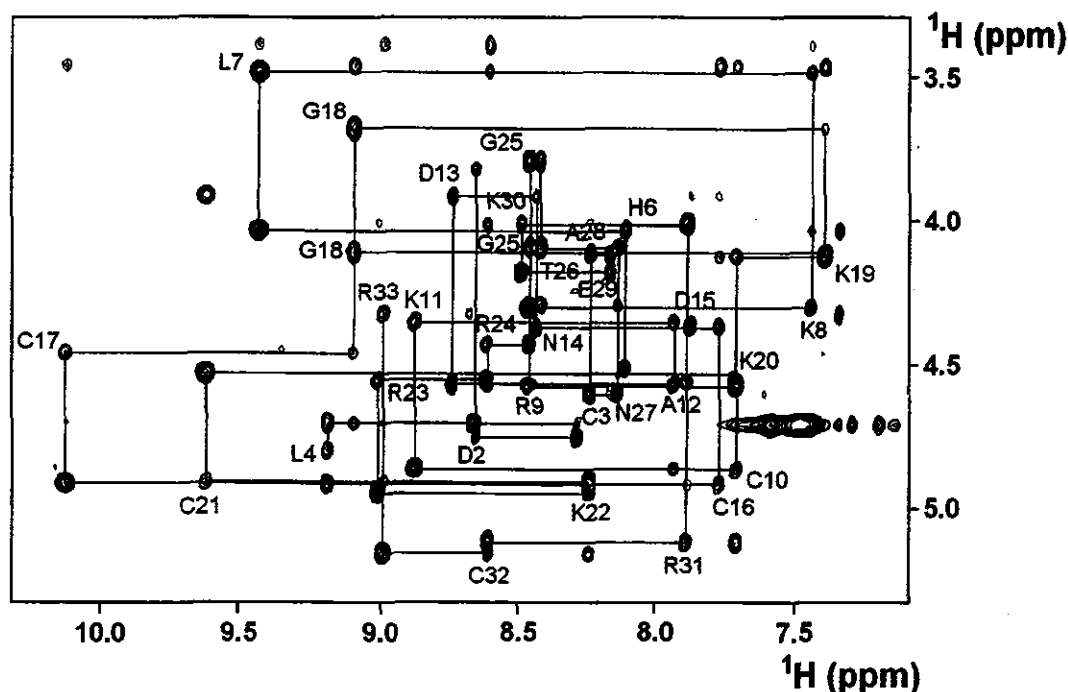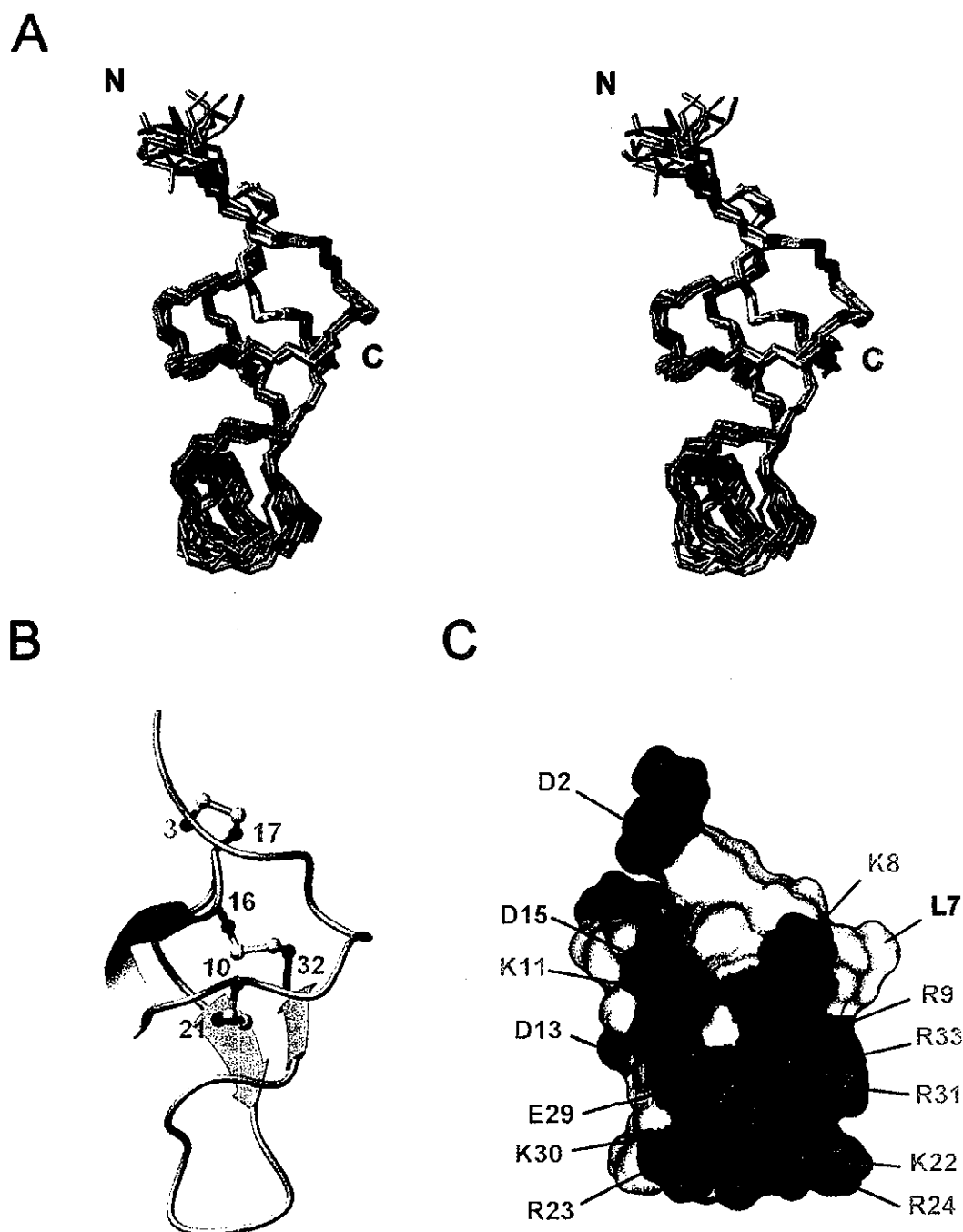

Figure 2   Sequential d_{αN}(i,i + 1) NOE connectivity for residues 2–33 in the NOESY spectrum observed with a mixing time of 300 ms

Intra-residue NH-C$^\alpha$H cross-peaks are labelled with the residue numbers by standard single-letter amino acid abbreviations.

A

B   C

Figure 3   Solution structure of wIpTx$_a$

(A) Stereo view of the heavy atom backbone (N, C$^\alpha$, C) for the 20 converged structures of wIpTx$_a$, which are superimposed for the best fit over the heavy atom backbone (residues Cys^3–Arg^{23} and residues Lys^{30}–Cys^{32}). Disulphide bonds are shown in yellow. (B) Schematic diagram of wIpTx$_a$ illustrating the location of the β-strands (cyan), 3$_{10}$-helical turn (red and yellow) and disulphide bonds (numbered ball and stick in yellow). These Figures were generated using the MOLMOL program [29]. (C) Surface profile of wIpTx$_a$. The molecular surface of wIpTx$_a$ is shown in colour according to the electrostatic potential (negatively charged amino acids are in red, positively charged amino acids are in blue, and uncharged or hydrophobic amino acids are in white). Residues D2, L7, K8, R9, K11, D13, D15, K22, R23, R24, E29, K30, R31 and R33 (single-letter amino acid codes) are indicated.

fingerprint region of the NOESY spectrum, containing sequential d$_{\alpha N}$($i,i + 1$) connectivity.

For the structure calculation of wIpTx$_a$, we used 473 distance constraints derived from the two-dimensional NOESY spectra, 25 dihedral angle constraints derived from the coupling constants and NOE measurements, 12 hydrogen-bond restraints derived from the hydrogen–deuterium exchange experiments

[Cys^{10}(HN)–Lys^{30}(CO), Lys^{20}(HN)–Arg^{33}(CO), Lys^{22}(HN)–Arg^{31}(CO), Arg^{31}(HN)–Lys^{22}(CO), Cys^{32}(HN)–Lys^8(CO) and Arg^{33}(HN)–Lys^{20}(CO)] and nine additional disulphide-bond restraints for a total of 519 restraints, corresponding to an average of 15.7 constraints per residue. The disulphide-bond pattern of synthetic wIpTx$_a$ was determined to be Cys^3–Cys^{17}, Cys^{10}–Cys^{21} and Cys^{16}–Cys^{32} by combined approaches of enzyme

Table 1   Structural statistics for the 20 lowest-energy structures

None of these 20 structures exhibited distance violations > 0.5 Å or dihedral angle violations > 5°.

Property	Value
RMS deviations from experimental distance constraints (Å) (494)*	0.0395 ± 0.0017
RMS deviations from experimental dihedral constraints (°) (25)*	0.7879 ± 0.1200
Energetic statistics (kcal · mol^{-1})†	
F_{NOE}	38.4861 ± 3.2228
F_{tor}	0.9821 ± 0.3076
F_{repel}	12.9477 ± 2.7362
E_{L-J}	−61.8040 ± 9.3520
RMS deviations from idealized geometry	
Bonds (Å)	0.0036 ± 0.0002
Angles (°)	0.6279 ± 0.0198
Impropers (°)	0.4603 ± 0.0350
Ramachandran analysis (residues 3–23 and 30–32)‡	
Most favoured regions	67.5%
Additionally allowed regions	31.6%
Generously allowed regions	0.9%
Disallowed regions	0%
Average RMSD (Å)	
Backbone (N, C^α, C) (residues 3–23 and 30–32)	0.38 ± 0.08
All heavy atoms (residues 3–23 and 30–32)	1.46 ± 0.26

* The number of each experimental constraint used in the calculations is given in parentheses.

† F_{NOE}, F_{tor} and F_{repel} are the energies related to the NOE violations, the torsion angle violations and the van der Waals repulsion term respectively. The values of the force constants used for these terms are the standard values as depicted in the X-PLOR 3.1 manual. E_{L-J} is the Lennard–Jones/van der Waals energy calculated with the CHARMm empirical energy function [56]. E_{L-J} was not used in the dynamic simulated annealing calculations.

‡ The program PROCHECK-NMR was used to assess the stereochemical quality of the structures.

fragmentation and chemical synthesis (C. W. Lee, E. H. Lee, T. Sasaki, K. Sato, K. Takeuchi, H. Takahashi, I. Shimada, D. H. Kim and J. I. Kim, unpublished work).

Structure description of wIpTx$_a$

Twenty structures with the lowest residual restraint violations were used to represent the three-dimensional structure of wIpTx$_a$ (Figure 3A). These structures have good non-bonded contacts as shown by low Lennard–Jones potential values, and a good covalent geometry, with only small deviations from the ideal bond lengths and bond angles (Table 1). There were no distance or dihedral angle restraint violations greater than 0.5 Å and 5° respectively. Excluding the final two residues of the N-terminus (Gly^1 and Asp^2) and the loop region from Arg^{24} to Glu^{29}, both of which were poorly defined by the NMR data, the average root mean square difference (RMSD) for the final 20 structures with respect to the mean co-ordinate positions was 0.38 ± 0.08 Å for the backbone atoms and 1.46 ± 0.26 Å for all heavy atoms. Structural statistics for the 20 converged structures of wIpTx$_a$ are summarized in Table 1.

The molecular structure of wIpTx$_a$ consists of two $β$-strands arranged in an antiparallel fashion, connected by four chain reversals (Figure 3B). The two $β$-strands are formed by residues Lys^{20}–Arg^{23} ($β$-strand I) and Lys^{30}–Arg^{33} ($β$-strand II). The first reversal occurs at residues Pro^5–Lys^8, which form a type IV $β$-turn (miscellaneous type). The second and third reversals occur at residues Asp^{13}–Asp^{15} and Cys^{16}–Lys^{19} and form a 3$_{10}$ helical turn and a type I $β$-turn respectively. Both of these are contained within the external long loop between the first turn and $β$-strand I. The final reversal occurs between residues Arg^{24} and Glu^{29} and

serves to reverse the backbone between $β$-strands I and II, without showing the characteristic distance pattern of a tight reverse turn. In terms of RMSD, this loop is poorly defined and presents the highest degree of structural disorder in the cysteine-rich region (Figure 3A).

The hydrophobic core of wIpTx$_a$ is entirely composed of the Cys^{10}, Cys^{16}, Cys^{21} and Cys^{32} side chains. The disulphide bond between Cys^{10} and Cys^{21} connects the second reversal to $β$-strand I, whereas the disulphide bonds between Cys^3 and Cys^{17} and between Cys^{16} and Cys^{32} connect the third reversal to the N-terminus and $β$-strand II respectively (Figure 3B). This pattern of disulphide connectivity is topologically classified as an 'inhibitor cystine knot' fold [34,35], in which the disulphide bond between Cys^{16} and Cys^{32} penetrates through a 13-residue ring formed by the peptide backbone and the other two disulphide bonds. Similar topology is frequently found in numerous toxic and inhibitory peptides, including the $ω$-conotoxins, $ω$-agatoxins and various protease inhibitors [36–42].

Structure–activity relationships of IpTx$_a$

The biological activities of synthetic wIpTx$_a$ and its 26 analogues were determined by examining their effects on RyR1 in SR vesicles from rabbit skeletal muscle, using a [^{3}H]ryanodine-binding assay. As shown in Figure 4, synthetic wIpTx$_a$ efficiently increased specific [^{3}H]ryanodine binding with EC$_{50}$ = 28.40 ± 6.71 nM and B$_{max}$ = 6.79 ± 0.30 pmol/mg of protein. The control binding of [^{3}H]ryanodine in the absence of wIpTx$_a$ was 0.57 ± 0.15 pmol/mg of protein. The specific [^{3}H]ryanodine binding in the presence of 30 nM of each analogue (corresponding to the apparent EC$_{50}$ of wIpTx$_a$) is summarized in Figure 4(A). Interestingly, all analogues possessing alanine replacements for basic residues caused an apparent reduction of specific [^{3}H]ryanodine binding, whereas all analogues possessing alanine replacements for acidic residues showed slight increases of specific [^{3}H]ryanodine binding. In addition, the H6A (His^6 → Ala), L7A, G25A (Gly^{25} → Ala), T26A (Thr^{26} → Ala) and N27A (Asn^{27} → Ala) analogues also showed decreased [^{3}H]ryanodine binding. These results suggest that a large surface area on IpTx$_a$ contributes to activating RyR1, and that the integrity of electrostatic potential, together with other additional factors, affects RyR1 activation.

In order to evaluate the residues essential to RyR1 activation in detail, we examined the dose-dependent activation by all synthetic IpTx$_a$ analogues further. The EC$_{50}$ values of all analogues are summarized in Table 2. Analysis of the dose effects showed that substituting residues at 16 positions, including positions 6, 7, 8, 9, 11, 19, 20, 22, 23, 24, 25, 26, 27, 30, 31 and 33 of IpTx$_a$ resulted in an important decrease of specific [^{3}H]ryanodine binding (Figures 4B, 4C and 4D). In particular, the R24A, R31A and R33A analogues completely abolished specific [^{3}H]ryanodine binding to RyR1. Other drastic decreases of specific [^{3}H]ryanodine binding were observed with L7A, K22A and R23A analogues (Figure 4D). In the case of acidic residues, alanine replacement resulted in slightly decreased EC$_{50}$ values, indicating that the negatively charged residues in IpTx$_a$ slightly obstruct the ability of the toxin molecule to activate RyR1. The CD spectral analyses showed that the conformations of the alanine-scanning analogues were almost identical with that of wIpTx$_a$ (Figure 1), except for the single case of the linear analogue (Ala^{3,10,16,17,21,32})IpTx$_a$, which displayed completely abolished activity (Figure 4D).

Previously, Gurrola et al. [17] reported that the mutations of Arg^{23} (R23E) and Thr^{26} (T26A and T26E) in IpTx$_a$ decreased the capacity of IpTx$_a$ to activate RyR1, and suggested that in IpTx$_a$, a
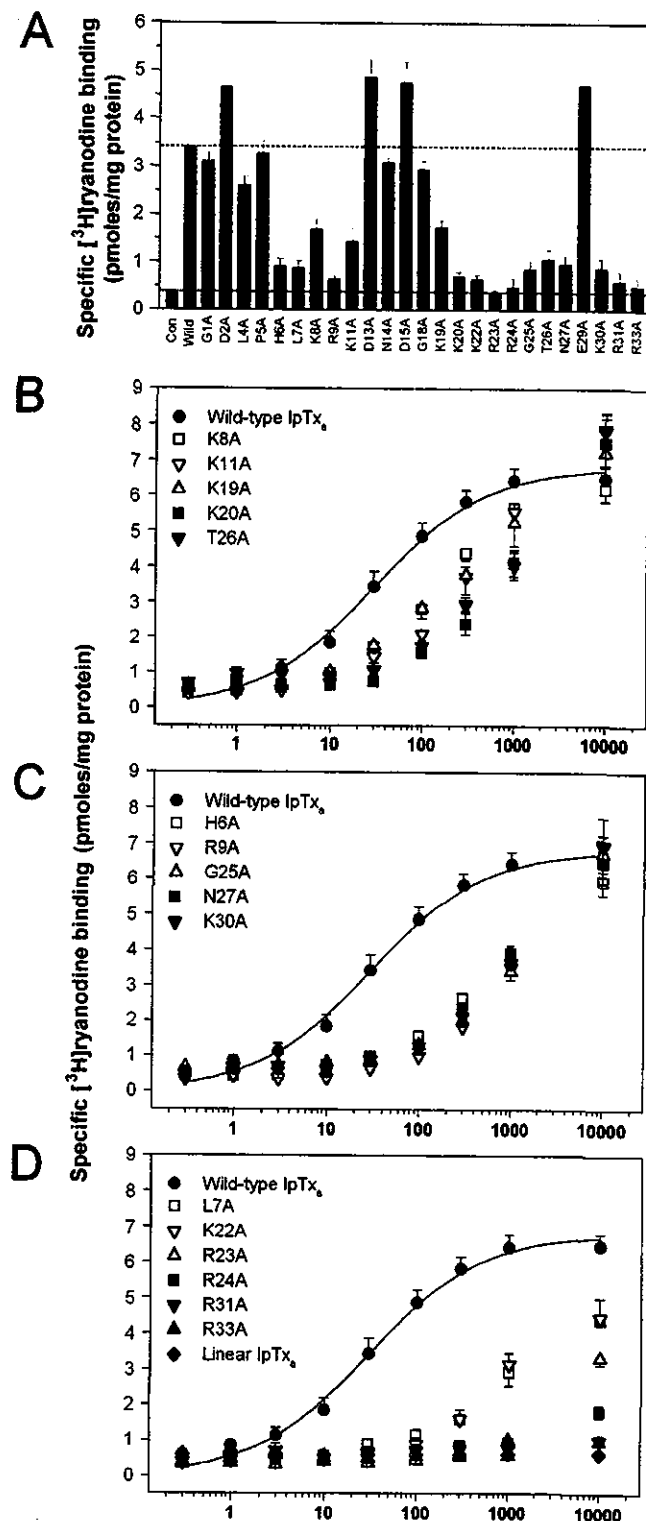
Figure 4   Activity measurements of wIpTx$_a$ and alanine-scanning analogues calculated with the [^{3}H]ryanodine binding assay

(A) Con and Wild are specific [^{3}H]ryanodine binding to RyR1 in the absence (0.38 ± 0.01 pmol/mg) and presence (3.44 ± 0.43 pmol/mg) of wIpTx$_a$ (30 nM) respectively. The values are the means ± S.E.M. of five independent experiments. (B)–(D) Dose-dependent activation of [^{3}H]ryanodine binding to RyR1 by wIpTx$_a$ and its analogues. The effect of wIpTx$_a$ on [^{3}H]ryanodine binding was compared with that of K8A, K11A, K19A, K20A and T26A (B), H6A, R9A, G25A, N27A and K30A (C), L7A, K22A, R23A, R24A, R31A, R33A and the linear analogue [(Ala^{3,10,16,17,21,32})IpTx$_a$] (D). The values are means ± S.E.M. of five independent replicates. Single-letter amino acid codes are used for the mutations.

Table 2   EC$_{50}$ values of wIpTx$_a$ and analogues

The data are means ± S.E.M. of five replicated experiments (see the Materials and methods section). + and − indicate the alanine-scanning analogue of positively and negatively charged residues of IpTx$_a$ respectively.

	Analogue	EC$_{50}$ (nM)
	Wild-type	28.40 ± 6.71
	G1A	33.40 ± 4.83
−	D2A	12.20 ± 2.17
	L4A	54.75 ± 7.79
	P5A	40.57 ± 5.18
	H6A	588.46 ± 71.24
	L7A	2769.22 ± 591.42
+	K8A	130.53 ± 15.97
+	R9A	727.58 ± 112.50
+	K11A	193.90 ± 34.72
−	D13A	9.21 ± 2.66
	N14A	32.25 ± 4.45
−	D15A	10.40 ± 1.05
	G18A	33.07 ± 5.14
+	K19A	140.97 ± 24.93
+	K20A	480.36 ± 92.21
+	K22A	1985.72 ± 383.56
+	R23A	11884.93 ± 2767.73
+	R24A	> 1 000 000
	G25A	680.52 ± 194.31
	T26A	327.12 ± 104.41
	N27A	570.52 ± 124.22
−	E29A	12.06 ± 1.30
+	K30A	615.88 ± 130.13
+	R31A	> 1 000 000
+	R33A	> 1 000 000
	Linear*	> 1 000 000

* Linear analogue [(Ala^{3,10,16,17,21,32})IpTx$_a$] was created by replacing all six cysteine residues with alanines.

cluster of basic residues (Lys^{19}–Arg^{24}) followed by Thr^{26} mimics the II–III loop of the DHPR α-subunit and is important for binding to RyR1. This agrees in part with our findings from analysis of analogues with alanine replacement of Arg^{23} and Thr^{26}. Through a series of dose-dependent experiments using a complete set of alanine-scanning analogues, however, we found that the most critical residues responsible for RyR1 activation (Arg^{24}, Arg^{31} and Arg^{33}, together with residues Lys^{22} and Arg^{23}) are located within the C-terminal region of IpTx$_a$. In addition, Leu^7 is of great importance, as it serves as a hydrophobic partner in the specific interaction with RyR1 (Figure 4D). The three-dimensional IpTx$_a$ structure shows that these six essential residues, together with other several important residues (His^6, Lys^8, Arg^9, Lys^{11}, Lys^{19}, Lys^{20}, Gly^{25}, Thr^{26}, Asn^{27} and Lys^{30}), are clustered together on one surface of the toxin molecule (an area of approx. 1900 Å^2) (Figure 5B). This region forms a functional surface with a putative binding site that probably interacts with the RyR1 cytoplasmic region. Interestingly, the opposite site is rich in acidic residues (Asp^2, Asp^{13}, Asp^{15} and Glu^{29}), and it forms a striking contrast with the positively charged functional surface (Figure 3C).

Structural comparisons with Mca and peptide A

In addition to IpTx$_a$, another exogenous ligand derived from scorpion venom mimics the effect of peptide A on RyR1. Mca, a 33-mer peptide toxin isolated from the venom of *Scorpio maurus*, activates RyR1 and shares 82% sequence identity with IpTx$_a$ [43]. As expected from this high degree of sequence identity,
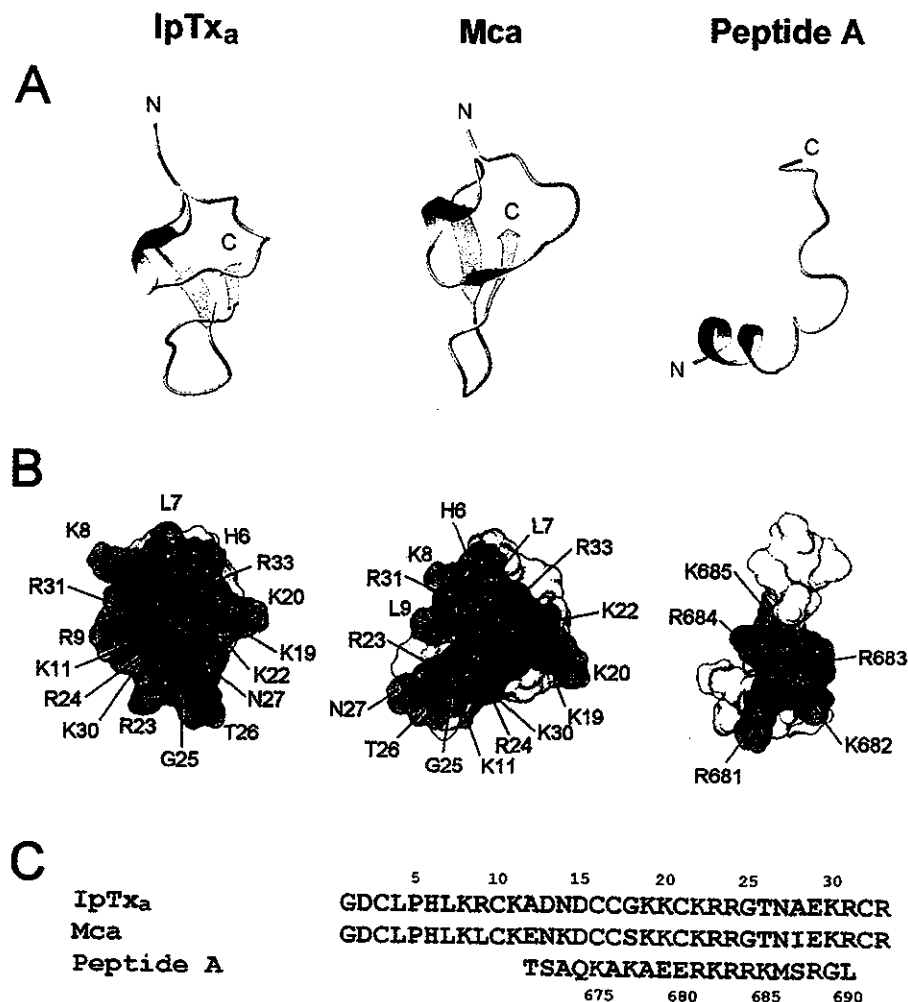
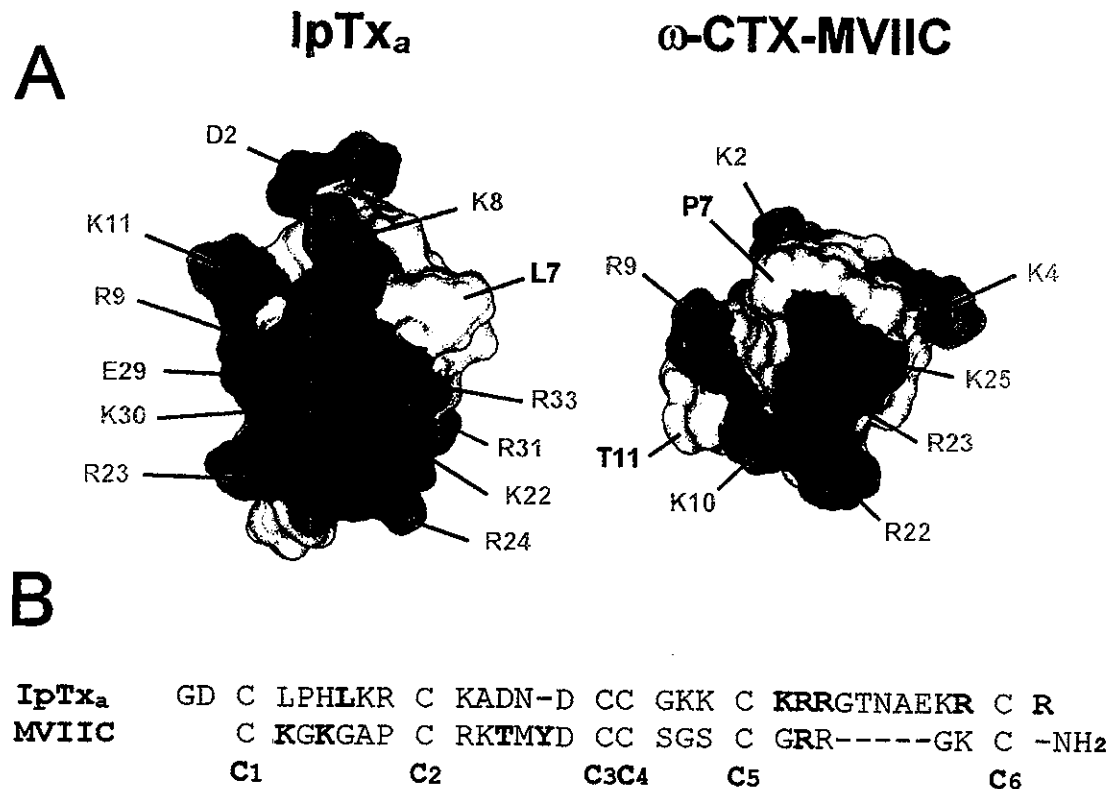**Figure 5   Structural comparison of IpTx$_a$, Mca (PDB code, 1C6W) and peptide A (PDB code, 1DU1)**

(A) Schematic diagrams of IpTx$_a$, Mca and peptide A illustrating the location of the β-strands (cyan) and 3$_{10}$-helical turn (red and yellow). (B) Surface profiles of IpTx$_a$, Mca and peptide A. For comparison, amino acids involved in the function of these peptides are emphasized in colour. Corresponding amino acids in Mca and peptide A, six essential amino acids (L7, K22, R23, R24, R31 and R33) of IpTx$_a$ and maurocalcine, and the R681–K685 region of peptide A are shown in purple; ten functionally important residues (H6, K8, R9, K11, K19, K20, G25, T26, N27 and K30) of IpTx$_a$ and maurocalcine are shown in green. Single-letter amino acid codes are used. (C) Comparative arrangements of the amino acid sequences of IpTx$_a$, Mca and peptide A.

both scorpion toxins present a similar overall molecular fold in solution. Mosbah et al. [44] determined the NMR solution structure of Mca, showing that it consists of three β-strands and four chain reversals. This report suggested that the three-dimensional surface of Mca has a unique charge distribution with a marked anisotropy that emerges from the molecule through its basic surface. Such a dipole moment is also observed in the surface profile of IpTx$_a$ (Figure 3C). IpTx$_a$ is the same length as Mca, and the two differ by only six amino acid residues: those at positions 9, 12, 13, 14, 18 and 28. Except for the Arg[9] residue, all residues of IpTx$_a$ that are important to RyR1 activation are well conserved in the primary and tertiary structures of Mca (Figure 5B), enclosing a slightly decreased functional surface area of approx. 1600 Å^2. Thus it would be reasonable to expect both scorpion toxins to have a similar binding affinity for a common site on RyR1 that is important for skeletal muscle E–C coupling. However, it should be noted that these scorpion toxins have different levels of effect on RyR1 gating, which undergoes a reversible transition between subconductance and fast gating states. Although both toxins may share a binding site on RyR1, IpTx$_a$ and Mca induce

subconductances that correspond to 28 % and 48 %, respectively, of the native full conductance at the positive holding potential [43,45]. This result seems to imply that a small change in the local charge distribution, due to variation of six amino acids, may induce slightly different substates in toxin gating of RyR1.

A major structural difference between IpTx$_a$ and Mca is found near the N-terminus, where Mca forms an additive peripheral β-strand (residues 9–11) that participates in the triple-stranded β-sheet (Figure 5A), but the corresponding sequence of IpTx$_a$ consists of only a single residue (Cys[10]) that is hydrogen-bonded to the central β-strand. Interestingly, the first residue (Leu[9]) of β-strand I in Mca joins with the side-chains of Cys[10], Cys[16], Cys[21] and Cys[32] to form the molecule's hydrophobic core. In IpTx$_a$, this residue is replaced by a positively charged arginine that plays a functional role in RyR1 activation. It is thus likely that some variations in amino acid sequences between IpTx$_a$ and Mca are to meet the structural and/or functional requirements of toxin molecules that evolve from different venomous sources.

In contrast, the solution conformation of the peptide A segment from the II–III loop of skeletal DHPR distinctly differs from that

Figure 6   Structural comparison of IpTx$_a$ and ω-CTX-MVIIC

(A) Comparison between surface profiles of IpTx$_a$ and ω-CTX-MVIIC (PDB code 1CNN). The colour codes are the same as those in Figure 3(C). The molecules are oriented with the positively charged amino acid cluster of each molecule in a certain plane. (B) Amino acids in the active sites of IpTx$_a$ and MVIIC are emboldened in their primary sequence alignments.

of IpTx$_a$ [46]. As shown in Figure 5(A), the structure of peptide A consists of a helical segment extending from the N-terminus to residue Lys^{685}, which is followed by a disordered region that extends through to the C-terminus. Despite this structural difference, these peptide activators show a distinct similarity in the spatial orientation of active residues necessary to target the common binding site on RyR1. It was previously reported that the peptide A-related segment (Glu^{666}–Leu^{690}) might bind to the same site as IpTx$_a$ on RyR1 [17]. In terms of competitive binding, peptide A presents a basic surface profile with the five consecutive residues (Arg^{681}–Lys^{685}) clustered at the C-terminal end of the α-helix, whereas IpTx$_a$ presents similar positively charged residues (Lys^{22}, Arg^{23}, Arg^{24}, Arg^{31} and Arg^{33}) aligned in a central region (Figure 5B). In both peptides, these basic surfaces are fully exposed to the solvent and present a characteristic shape that may be directly involved in the RyR1 activation important for skeletal muscle E–C coupling. Together, these observations may explain, at least in part, how IpTx$_a$ and peptide A compete for a common binding site on the RyR1 channel protein.

However, although both use a common binding site, the affinities of IpTx$_a$ and peptide A for RyR1 differ. IpTx$_a$ activates RyR1 with a high nanomolar affinity, whereas peptide A activates RyR1 with a lower micromolar affinity [17]. As summarized in Table 2, the EC$_{50}$ values for the IpTx$_a$ alanine-scanning analogues varied considerably depending on the location of the substitution. [^{3}H]Ryanodine binding to RyR1 was significantly reduced following alanine replacement of all tested basic residues, including the five critical residues (Lys^{22}, Arg^{23}, Arg^{24}, Arg^{31} and Arg^{33}), and several other residues (His^6, Leu^7, Gly^{25}, Thr^{26} and Asn^{27}), indicating that amino acid residues involved in RyR1

activation make up over the half of the toxin molecule with the exception of cysteine residues. In contrast, the functional surface of peptide A includes only five consecutive basic residues (Arg^{681}, Lys^{682}, Arg^{683}, Arg^{684} and Lys^{685}) that are clustered at the C-terminal end of the α-helix. In three dimensions, IpTx$_a$ exhibits a large functional surface area, approx. 1900 Å^2, whereas peptide A bears a much smaller functional surface area, approx. 800 Å^2.

In measurements of single channel currents, IpTx$_a$ induced a long-lived subconductance state in RyR1 that possessed 28 % of the characteristic full open state at the positive holding potential. In contrast, peptide A induced long-lived channel closures with occasional burst transitions to subconductance states of 65 % or 86 % of the full conductance, indicating that IpTx$_a$ and peptide A stabilize distinct RyR1 gating states through somewhat different interaction mechanisms [47].

Overall, these results suggest that the site where peptide A binds to RyR1 belongs to a subset of macrosites capable of being occupied by IpTx$_a$, resulting in differing the affinity and the mode of activation.

Structural comparison with ω-CTX-MVIIC, a voltage-gated P/Q-type Ca^{2+} channel blocker

Voltage-gated Ca^{2+} channels are classified into several subtypes, which include the L-, N-, P-, Q-, R- and T-subtypes, according to their electrophysiological and pharmacological properties [48]. ω-CTXs are highly potent blockers of voltage-gated Ca^{2+} channels and are useful ligands for the pharmacological discrimination of Ca^{2+} channel subtypes [49]. Extensive structure–activity

studies have revealed that all ω-CTXs (e.g. ω-CTX-GVIA and -MVIIA, N-type Ca^{2+}-channel blockers, and the ω-CTX-MVIIC, P/Q-type Ca^{2+}-channel blocker) share significant structural similarity in three dimensions, but possess distinct functional sites responsible for the specific interaction with individual voltage-gated Ca^{2+} channel subtypes [50–53]. The molecular architecture of the cone-snail ω-CTXs is entirely composed of an 'inhibitor cystine knot' fold constrained by three intramolecular disulphide bonds. This structure is also found in the RyR1-targeting scorpion toxins IpTx$_a$ and Mca, indicating that the ω-scaffold is a general molecular topology of exogenous toxins targeting the Ca^{2+} channels.

Among ω-CTXs, ω-CTX-MVIIC is the most structurally similar to the scorpion RyR1 activators. As shown in Figure 6(A), ω-CTX-MVIIC exhibits a highly basic structural surface that includes several positively charged amino acid residues. Although there is a high degree of structural similarity between IpTx$_a$ and ω-CTX-MVIIC, the two Ca^{2+}-channel-targeting toxins show no cross-reactivity; IpTx$_a$ has no affinity for the P/Q-type Ca^{2+} channel and ω-CTX-MVIIC has no affinity for the RyR1 [17]. This suggests that the two toxins form distinct functional sites responsible for the specific interaction with each channel protein [53]. The functionally important residues of IpTx$_a$ for the binding to RyR1 consist of five protruding basic residues (Lys^{22}, Arg^{23}, Arg^{24}, Arg^{31} and Arg^{33}) and one hydrophobic residue (Leu^7), with approx. ten additional residues assisting. In contrast, the functional residues for ω-CTX-MVIIC action on the P/Q-type Ca^{2+} channel include three basic residues (Lys^2, Lys^4 and Arg^{22}) and two polar residues (Thr^{11} and Tyr^{13}) [53], suggesting that IpTx$_a$ forms a larger functional surface than does ω-CTX-MVIIC. ω-CTX-MVIIC is shorter in length than IpTx$_a$, and its positively charged surface area is also smaller than that of IpTx$_a$, mainly due to fewer basic amino acids between the fifth cysteine and the C-terminus (three compared with six) (Figure 6B). In IpTx$_a$, this region forms a long hairpin loop with an electropositive potential, incorporating β-strands I and II (Figure 3B). As previously mentioned, both IpTx$_a$ and peptide A share a necessary alignment of five basic residues that act at a common site on RyR1 (Figure 5B). ω-CTX-MVIIC also possesses a similar basic structural region, consisting of five basic residues (Arg^9, Lys^{10}, Arg^{22}, Arg^{23} and Lys^{25}) (Figure 6A), but its shape is relatively different from that of both IpTx$_a$ and peptide A, resulting in a failure to activate RyR1. Taken together, these observations suggest that the correct distribution of surface charges is important to specific interaction with RyR1, rather than the globular structure maintained by the conserved disulphide framework. This may be one reason why ω-CTX-MVIIC does not compete for the same binding site as IpTx$_a$ and peptide A, thus providing structural and molecular insights into the specific interaction mode of RyR1-targeting peptide effectors.

Conclusion

In the present study, we have determined the NMR solution structure of the peptide activator IpTx$_a$, and identified the functional surface that is responsible for its high-affinity interaction with RyR1. A detailed comparison between IpTx$_a$ and peptide A revealed that the existence of complementary surface profiles, created by different molecular scaffolds, is limited between the C-terminal β-sheet region of IpTx$_a$ and the α-helical end region of peptide A. Thus it seems that the site where peptide A binds to RyR1 belongs to a subset of the macrosites occupied by IpTx$_a$, resulting in differing affinities and subconductance states. A comparative surface analysis with ω-CTX-MVIIC suggests that the

characteristic shape of positively charged binding surface rather than globular shape is responsible for the specific interaction of RyR1-targeting peptide effectors. Taken together, these structural and functional studies on ryanodine-sensitive channel effectors, together with our knowledge of the three-dimensional structure of DHPR and RyR1 obtained previously by cryo-electron microscopy and image processes [54,55], open up a new avenue for the elucidation of the molecular details of skeletal type E–C coupling.

REFERENCES

1   Bers, D. M. (1991) Excitation–Contraction Coupling and Cardiac Contractile Force, Kluwer Academic Publishers, Dordrecht

2   Nabauer, M., Callewaert, G., Cleemann, L. and Morad, M. (1989) Regulation of calcium release is gated by calcium current, not gating charge, in cardiac myocytes. Science **244**, 800–803

3   Armstrong, C. M., Bezanila, F. M. and Horowicz, P. (1972) Twitches in the presence of ethylene glycol bis(-aminoethyl ether)-N,N′-tetracetic acid. Biochim. Biophys. Acta **267**, 605–608

4   Marty, I., Robert, M., Villaz, M., De Jongh, K. S., Lai, Y., Catterall, W. A. and Ronjat, M. (1994) Biochemical evidence for a complex involving dihydropyridine receptor and ryanodine receptor in triad junctions of skeletal muscle. Proc. Natl. Acad. Sci. U.S.A. **91**, 2270–2274

5   Tanabe, T., Beam, K. G., Adams, B. A., Niidome, T. and Numa, S. (1990) Regions of the skeletal muscle dihydropyridine receptor critical for excitation–contraction coupling. Nature (London) **346**, 567–569

6   Lu, X., Xu, L. and Meissner, G. (1994) Activation of the skeletal muscle calcium release channel by a cytoplasmic loop of the dihydropyridine receptor. J. Biol. Chem. **269**, 6511–6516

7   El-Hayek, R., Antoniu, B., Wang, J., Hamilton, S. L. and Ikemoto, N. (1995) Identification of calcium release-triggering and blocking regions of the II–III loop of the skeletal muscle dihydropyridine receptor. J. Biol. Chem. **270**, 22116–22118

8   Nakai, J., Dirksen, R. T., Nguyen, H. T., Pessah, I. N., Beam, K. G. and Allen, P. D. (1996) Enhanced dihydropyridine receptor channel activity in the presence of ryanodine receptor. Nature (London) **380**, 72–75

9   Slavik, K. J., Wang, J. P., Aghdasi, B., Zhang, J. Z., Mandel, F., Malouf, N. and Hamilton, S. L. (1997) A carboxy-terminal peptide of the α1-subunit of the dihydropyridine receptor inhibits Ca^{2+} release channels. Am. J. Physiol. **272**, C1475–C1481

10 Leong, P. and MacLennan, D. H. (1998) The cytoplasmic loops between domains II and III and domains III and IV in the skeletal muscle dihydropyridine receptor bind to a contiguous site in the skeletal muscle ryanodine receptors. J. Biol. Chem. **273**, 29958–29964

11 Grabner, M., Dirksen, R. T., Suda, N. and Beam, K. G. (1999) The II–III loop of the skeletal muscle dihydropyridine receptor is responsible for the bi-directional coupling with the ryanodine receptor. J. Biol. Chem. **274**, 21913–21919

12 Sencer, S., Papineni, R. V., Halling, D. B., Pate, P., Krol, J., Zhang, J. Z. and Hamilton, S. L. (2001) Coupling of RYR1 and L-type calcium channels via calmodulin binding domains. J. Biol. Chem. **276**, 38237–38241

13 Nakai, J., Sekiguchi, N., Rando, T. A., Allen, P. D. and Beam, K. G. (1998) Two regions of the ryanodine receptor involved in coupling with L-type Ca^{2+} channels. J. Biol. Chem. **273**, 13403–13406

14 El-Hayek, R., Lokuta, A. J., Arevalo, C. and Valdivia, H. H. (1995) Peptide probe of ryanodine receptor function. J. Biol. Chem. **270**, 28696–28704

15 Zamudio, F. Z., Gurrola, G. B., Arevalo, C., Sreekumar, R., Walker, J. W., Valdivia, H. H. and Possani, L. D. (1997) Primary structure and synthesis of imperatoxin A (IpTx$_a$), a peptide activator of Ca^{2+} release channels/ryanodine receptors. FEBS Lett. **405**, 385–389

16 El-Hayek, R. and Ikemoto, N. (1998) Identification of the minimum essential region in the II–III loop of the dihydropyridine receptor 1 subunit required for activation of skeletal muscle-type excitation–contraction coupling. Biochemistry **37**, 7015–7020

17 Gurrola, G. B., Arevalo, C., Sreekuma, R., Lokuta, A. J., Walker, J. W. and Valdivia, H. H. (1999) Activation of ryanodine receptors by imperatoxin A and a peptide segment of the II–III loop of the dihydropyridine receptor. J. Biol. Chem. **274**, 7879–7886

18 Green, D., Pace, S., Curtis, S. M., Sakowska, M., Lamb. G. D., Dulhunty, A. F. and Casarotto, M. G. (2003) The three-dimensional structural surface of two β-sheet scorpion toxins mimics that of an α-helical dihydropyridine receptor segment. Biochem. J. **370**, 517–527

19 Rance, M., Sørensen, O. W., Bodenhausen, G., Wagner, G., Ernst, R. R. and Wüthrich, K. (1983) Improved spectral resolution in COSY ^{1}H NMR spectra of protein via double quantum filtering. Biochem. Biophys. Res. Commun. **117**, 479–485

20 Griesinger, C., Sørensen, O. W. and Ernst, R. R. (1987) Practical aspects of the E.COSY technique: measurement of scalar spin–spin coupling constants in peptides. J. Magn. Reson. **75**, 474–492

21 Bax, A. and Davis, D. G. (1985) MLEV-17-based two-dimensional homonuclear magnetization transfer spectroscopy. J. Magn. Reson. **65**, 355–360

22 Jeener, J., Meier, B. N., Bachmann, P. and Ernst, R. P. (1979) Investigation of exchange processes by two-dimensional NMR spectroscopy. J. Chem. Phys. **71**, 4546–4553

23 Wüthrich, K., Billeter, M. and Braun, W. (1983) Pseudo-structures for the 20 common amino acids for use in studies of protein conformations by measurement of intramolecular proton–proton distance constraints with nuclear magnetic resonance. J. Mol. Biol. **169**, 949–961

24 Clore, M., Gronenborn, A. M., Nilges, M. and Ryan, C. A. (1987) Three-dimensional structure of potato carboxypeptidase inhibitor in solution: a study using nuclear magnetic resonance, distance geometry and restraint molecular dynamics. Biochemistry **26**, 8012–8023

25 Nilges, M., Gronenborn, A. M., Brünger, A. T. and Clore, G. M. (1988) Determination of three-dimensional structures of proteins by simulated annealing with interproton distance restraints: application to crambin, potato carboxypeptidase inhibitor and barley serine proteinase inhibitor 2. Protein Eng. **2**, 27–38

26 Brünger, A. T. (1993) X-PLOR Manual, Version 3.1, Yale University, New Haven

27 Laskowski, R. A., Rullmann, J. A., MacArthur, M. W., Kaptein, R. and Thornton, J. M. (1996) AQUA and PROCHECK-NMR: programs for checking the quality of protein structures solved by NMR. J. Biomol. NMR **8**, 477–486

28 Hutchinson, E. G. and Thornton, J. M. (1996) PROMOTIF – a program to identify and analyze structural motifs in proteins. Protein Sci. **5**, 212–220

29 Koradi, R., Billeter, M. and Wüthrich, K. (1996) MOLMOL: a program for display and analysis of macromolecular structures. J. Mol. Graph. **14**, 29–32

30 Kim, D. H., Sreter, F. A., Ohnishi, S. T., Ryan, J. F., Roberts, J., Allen, P. D., Meszaros, L. G., Antonia, B. and Ikemoto, N. (1984) Kinetic studies of Ca^{2+} release from sarcoplasmic reticulum of normal and malignant hyperthermia susceptible pig muscles. Biochim. Biophys. Acta **775**, 320–327

30a Bradford, M. M. (1976) A rapid and sensitive method for the quantitation of microgram quantities of protein utilizing the principle of protein-dye binding. Anal. Biochem. **72**, 248–254

31 Campbell, K. P., Knudson, C. M., Imagawa, T., Leung, A. T., Sutko, J. L., Kahl, S. D., Raab, C. R. and Madson, L. (1987) Identification and characterization of the high affinity [^{3}H]ryanodine receptor of the junctional sarcoplasmic reticulum Ca^{2+} release channel. J. Biol. Chem. **262**, 6460–6463

32 Kim, D. H., Mkparu, F., Kim, C. R. and Caroll, R. F. (1994) Alteration of Ca^{2+} release channel function in sarcoplasmic reticulum of pressure-overload-induced hypertrophic rat heart. J. Moi. Cell. Cardiol. **26**, 1505–1512

33 Wüthrich, K. (1986). NMR of Proteins and Nucleic Acids, John Wiley and Sons, Inc., New York

34 Pallaghy, P. K., Nielsen, K. J., Craik, D. J. and Norton, R. S. (1994) A common structural motif incorporating a cystine knot and a triple-stranded β-sheet in toxic and inhibitory polypeptides. Protein Sci. **3**, 1833–1839

35 Norton, R. S. and Pallaghy, P. K. (1998) The cystine knot structure of ion channel toxins and related polypeptides. Toxicon **36**, 1573–1583

36 Davis, J. H., Bradley, E. K., Miljanich, G. P., Nadasdi, L., Ramachandran, J. and Basus, V. J. (1993) Solution structure of omega-conotoxin GVIA using 2-D NMR spectroscopy and relaxation matrix analysis. Biochemistry **32**, 7396–7405

37 Pallaghy, P. K., Duggan, B. M., Pennington, M. W. and Norton, R. S. (1993) Three-dimensional structure in solution of the calcium channel blocker ω-conotoxin. J. Mol. Biol. **234**, 405–420

38 Kohno, T., Kim, J. I., Kobayashi, K., Kodera, Y., Maeda, T. and Sato, K. (1995) Three-dimensional structure in solution of the calcium channel blocker ω-conotoxin MVIIA. Biochemistry **34**, 10256–10265

39 Kim, J. I., Konishi, S., Iwai, H., Kohno, T., Gouda, H., Shimada, I., Sato, K. and Arata, Y. (1995) Three-dimensional solution structure of the calcium channel antagonist ω-agatoxin IVA: consensus molecular folding of calcium channel blockers. J. Mol. Biol. **250**, 659–671

40 Reily, M. D., Thanabal, V. and Adams, M. E. (1995) The solution structure of ω-Aga-IVB, a P-type calcium channel antagonist from venom of the funnel web spider, Agelenopsis aperta. J. Biomol. NMR **5**, 122–132

41 Saether, O., Craik, D. J., Campbell, I. D., Sletten, K., Juul, J. and Morman, D. G. (1995) Elucidation of the primary and three-dimensional structure of the uterotonic polypeptide kalata B1. Biochemistry **34**, 4147–4158

42 Nilges, M., Habazettl, J., Brünger, A. T. and Holak, T. A. (1991) Relaxation matrix refinement of the solution structure of squash trypsin inhibitor. J. Mol. Biol. **248**, 106–124

43 Fajloun, Z., Kharrat, R., Chen, L., Lecomte, C., Di Luccio, E., Bichet, D., El Ayeb, M., Rochat, H., Allen, P. D., Pessah, I. N. et al. (2000) Chemical synthesis and characterization of maurocalcine, a scorpion toxin that activates Ca^{2+} release channel/ryanodine receptors. FEBS Lett. **469**, 179–185

44 Mosbah, A., Kharrat, R., Fajloun, Z., Renisio, J. G., Blanc, E., Sabatier, J. M., El Ayeb, M. and Darbon, H. (2000) A new fold in the scorpion toxin family, associated with an activity on a ryanodine-sensitive calcium channel. Proteins **40**, 436–442

45 Tripathy, A., Resch, W., Xu, L., Valdivia, H. H. and Meissner, G. (1998) Imperatoxin A induces subconductance states in Ca^{2+} release channels (ryanodine receptors) of cardiac and skeletal muscle. J. Gen. Physiol. **111**, 679–690

46 Casarotto, M. G., Gibson, F., Pace, S. M., Curtis, S. M., Mulcair, M. and Dulhunty, A. F. (2000) A structural requirement for activation of skeletal ryanodine receptors by peptides of the dihydropyridine receptor II–III loop. J. Biol. Chem. **275**, 11631–11637

47 Chen, L., Esteve, E., Sabatier, J. M., Ronjat, M., Waard, M. D., Allen, P. D. and Pessah, I. N. (2003) Maurocalcine and peptide A stabilize distinct subconductance states of ryanodine receptor type 1 (RyR1) revealing a proportional gating mechanism. J. Biol. Chem. **278**, 16095–16106

48 Snutch, T. P. and Reiner, P. B. (1992) Ca^{2+} channels: diversity of form and function. Curr. Opin. Neurobiol. **2**, 247–253

49 Olivera, B. M., Miljanich, G. P., Ramachandran, J. and Adams, M. E. (1994) Calcium channel diversity and neurotransmitter release: the ω-conotoxins and ω-agatoxins. Annu. Rev. Biochem. **63**, 823–867

50 Kim, J. I., Takahashi, M., Ogura, A., Kohno, T., Kudo, Y. and Sato, K. (1994) Hydroxyl group of Tyr^{13} is essential for the activity of ω-conotoxin GVIA, a peptide toxin for N-type calcium channel. J. Biol. Chem. **269**, 23876–23878

51 Kim, J. I., Takahashi, M., Ohtake, A., Wakamiya, A. and Sato, K. (1995) Tyr^{13} is essential for the activity of ω-conotoxin MVIIA and GVIA, specific N-type calcium channel blockers. Biochem. Biophys. Res. Commun. **206**, 449–454

52 Kim, J. I., Takahashi, M., Martin-Moutot, N., Seagar, M. J., Ohtake, A. and Sato, K. (1995) Tyr^{13} is essential for the binding of ω-conotoxin MVIIC to the P/Q-type calcium channel. Biochem. Biophys. Res. Commun. **214**, 305–309

53 Sato, K., Raymond, C., Martin-Moutot, N., Sasaki, T., Ohtake, A., Minami, K., Van Renterghem, C., Kim, J. I., Takahashi, M. and Seagar, M. J. (2000) Binding of Ala-scanning analogs of ω-conotoxin MVIIC to N- and P/Q-type calcium channels. FEBS Lett. **469**, 147–150

54 Samso, M., Trujillo, R., Gurrola, G. B., Valdivia, H. H. and Wagenknecht, T. (1999) Three-dimensional location of the imperatoxin A binding site on the ryanodine receptor. J. Cell Biol. **146**, 493–499

55 Serysheva, I. I., Ludtke, S. J., Baker, M. R., Chiu, W. and Hamilton, S. L. (2002) Structure of the voltage-gated L-type Ca^{2+} channel by electron cryomicroscopy. Proc. Natl. Acad. Sci. U.S.A. **99**, 10370–10375

56 Brooks, B. R., Bruccoleri, R. E., Olafson, B. D., States, D. J., Swaminathan, S. and Karplus, M. (1983) CHARMm: a program for macromolecular energy, minimization, and dynamics calculations. J. Comput. Chem. **4**, 187–217

Adenosine A_1-receptor-mediated tonic inhibition of glutamate release at rat hippocampal CA3–CA1 synapses is primarily due to inhibition of N-type Ca^{2+} channels

Satoshi Manita[a], Yoshinobu Kawamura[a], Kazuki Sato[b], Masashi Inoue[a], Yoshihisa Kudo[a], Hiroyoshi Miyakawa[a],*

[a]Laboratory of Cellular Neurobiology, School of Life Science, Tokyo University of Pharmacy and Life Science, Hachioji, Tokyo 192-0392, Japan
[b]Faculty of Human Environmental Science, Fukuoka Women's University, Kasumigaoka, Higashi-ku, Fukuoka 813-8529, Japan

Abstract

The voltage-gated Ca^{2+} channels responsible for synaptic transmission at CA3–CA1 synapses are mainly P/Q- and N-types. It has been shown that tonic inhibition of transmission due to activation of adenosine A_1 receptors occurs at this synapse. We have recently developed a technique to monitor synaptically released glutamate which is based on synaptically induced glial depolarisation. Using this technique, we have examined the effects of different voltage-gated Ca^{2+} channel blockers on glutamate release. Under conditions in which the adenosine A_1 receptor was not blocked, ω-AgaIVA (a P/Q-type voltage-gated Ca^{2+} channel blocker) suppressed synaptically induced glial depolarisation to a greater extent than ω-CgTxGVIA (an N-type voltage-gated Ca^{2+} channel blocker) did. In contrast, in the presence of an adenosine A_1 receptor antagonist, ω-AgaIVA was less effective at suppressing synaptically induced glial depolarisation than ω-CgTxGVIA. These results indicate that, in the absence of adenosine A_1 receptor-mediated tonic inhibition, the contribution of N-type is much greater than that of P-type, and that N-types are the primary target of tonic inhibition in normal conditions in which adenosine A_1 receptor-mediated tonic inhibition is present.
© 2004 Elsevier B.V. All rights reserved.

Keywords: Presynaptic terminal; Ca^{2+} channel; Adenosine receptor; Hippocampus

1. Introduction

Transmitter release at presynaptic terminals is one of the major targets for neuromodulation (Vizi, 2000). For example, it has been shown that activation of presynaptic receptors, such as metabotropic glutamate (Cartmell and Schoepp, 2000), adenosine A_1 (Dunwiddie and Masino, 2001), gamma-aminobutyric acid $(GABA)_B$ (Misgeld et al., 1995) and muscarinic and cannabinoid (Schlicker and Kathmann, 2001) receptors, modulates transmitter release at hippocampal CA3–CA1 synapses, and that inhibition of voltage-gated Ca^{2+} channels in the presynaptic terminals

can be responsible for this modulation (Ambrosio et al., 1997; Mogul et al., 1993; Wu and Saggau, 1997).

Various studies have shown that N- and P/Q-type channels are responsible for glutamate release at CA3–CA1 synapses in the rat hippocampus (Luebke et al., 1993; Takahashi and Momiyama, 1993; Wheeler et al., 1994; Wu and Saggau, 1994b, 1997; Reuter, 1995; Reuter, 1996). Measuring Ca^{2+}-dependent [³H]glutamate release from hippocampal synaptosomes using biochemical techniques, Luebke et al. (1993) reported that P-type channels play a more prominent role than N-type channels. Takahashi and Momiyama (1993) showed that excitatory postsynaptic currents in hippocampal CA1 neurons in slice preparations are suppressed to a greater extent by ω-AgaIVA, a P-type channel blocker, than by ω-CgTxGVIA, an N-type channel

blocker (84% and 31% suppression, respectively). This finding was confirmed by Wheeler et al. (1994), who showed that the slope of the field excitatory post synaptic potential (fEPSP) at synapses from CA3 to CA1 pyramidal neurons in the hippocampus is reduced by ω-AgaIVA to a greater extent than by ω-CgTxGVIA (85% and 46%, respectively). Wu and Saggau (1994b) performed fast Ca^{2+} imaging of presynaptic terminals at rat CA3–CA1 synapses and reported that application of N- or P/Q-type channel blockers reduces presynaptic Ca^{2+} influxes by 21% or 35%, respectively. These studies showed that the contribution of P/Q-type channels is greater than that of N-type channels. In contrast, Reuter (1995) reported that, in rat hippocampal cell cultures, the exocytosis of the styryl dye, FM1-43, from synaptic vesicles during synaptic transmission following Ca^{2+} entry through Ca^{2+} channels is inhibited by ω-CgTxGVIA to a greater extent than by ω-AgaIVA.

However, most of the above studies were performed under conditions in which glutamate release from presynaptic terminals might have been suppressed by the action of various modulators. For example, Wu and Saggau (1994a) reported that the adenosine A_1 antagonist, 8-cyclopentyl-1,3-dipropylxanthine (8-CPT), enhances both the presynaptic Ca^{2+} rise and the fEPSP, suggesting tonic inhibition by endogenous adenosine. It has been reported that adenosine suppress transmitter release by inhibiting voltage-gated Ca^{2+} channels (Dunwiddie and Masino, 2001). In order to determine which types of voltage-gated Ca^{2+} channels are responsible for transmitter release, it is necessary to compare contribution of voltage-gated Ca^{2+} channels in the absence of tonic inhibition.

Several different methods, such as the measurement of postsynaptic responses and presynaptic $[Ca^{2+}]_i$ changes, have been used to investigate the contribution of voltage-gated Ca^{2+} channels to transmitter release. However, these methods are rather indirect, as voltage-gated Ca^{2+} channels may be involved in determining postsynaptic responses and as there may be presynaptic $[Ca^{2+}]_i$ changes that do not contribute to transmitter release. We have recently developed a novel optical method to monitor synaptically induced glutamate release which involves detecting the depolarisation of glial cells caused by glutamate uptake using a voltage-sensitive dye and a fast optical imaging system (Kojima et al., 1999). In the present study, we monitored glutamate release at CA3–CA1 synapses in rat hippocampal slice preparations by using this method in the absence of adenosine-mediated tonic inhibition and examined the effects of specific blockers of N- and P/Q-type channels. We have confirmed that glutamate release is tonically inhibited by activation of adenosine A_1 receptors and demonstrated that, in the absence of inhibition, the contribution of N-type channels is greater than that of P/Q-type channels. Thus, N-type channels are the major target of the adenosine A_1 receptor-mediated inhibitory effect on transmission at CA3–CA1 synapses.

2. Materials and methods

The experimental protocols were approved by the Institutional Animal Care and Use Committee of the Tokyo University of Pharmacy and Life Science, and were carried out in accordance with the National Institute of Health Guide for the Care and Use of Laboratory Animals.

2.1. Slice preparation

Hippocampal slices were prepared from 3-week-old male Wistar rats. The animals were decapitated under deep diethyl ether anaesthesia, and the brains removed and rapidly cooled in artificial cerebrospinal fluid [composition (in mM): 110 choline chloride for preparing slices or 124 NaCl for experiments, 2.5 KCl, 26 $NaHCO_3$, 10 glucose, 1.25 NaH_2PO_4, 2 $CaCl_2$ and 1 $MgCl_2$, pH 7.4] bubbled continuously with a gas mixture of 95% O_2 and 5% CO_2. Slices (400 μm thick) were prepared using a rotary slicer (Dosaka EM model DTY-7700, Japan).

2.2. Voltage-sensitive dye measurement

The method has been described in detail elsewhere (Kojima et al., 1999). Briefly, slices were maintained in a holding chamber for at least 30 min, then stained with the voltage-sensitive dye, RH155 (NK3041) (Molecular Probes, Eugene, OR, or Nippon Kankoh-Shikiso, Okayama, Japan) by submersion for 30 min in artificial cerebrospinal fluid containing 0.21 mg/ml of RH155. The stained slices were placed in an experimental chamber mounted on an inverted microscope (TMD-300, Nikon, Tokyo, Japan) and changes in dye absorption, which are related to the change in membrane potential, were measured at 700 nm using a high-speed (maximum frame rate 2 kHz) 16×16 photodiode array system (Agrus-50/PDA, Hamamatsu Photonics, Hamamatsu, Japan). The photo-currents generated at the photodiodes were converted to voltage using a current-to-voltage converter with a 50 MΩ feedback resistor and the data transferred to a sample-and-hold device, then DC-coupled to a 16 bit resolution analogue-to-digital converter. All optical signals were displayed as changes in light intensity divided by the total light intensity ($\Delta I/I$). In most experiments, a ×10 objective lens (NA 0.45) was used; in this case, each diode imaged an area of 52.5×52.5 μm. Experiments were performed at 24–28 °C. Synaptic responses were evoked by delivering a short current pulse of 200 μs duration using a bipolar tungsten electrode placed in the stratum radiatum to stimulate Schaffer collaterals. The stimulus was applied every 5 s and the optical signals averaged over 9–12 trials. To record extracellular field potentials, glass pipettes (1.5×90 mm, 1–5 MΩ) filled with artificial cerebrospinal fluid were inserted into the stratum radiatum. The potentials were amplified by a high-gain AC amplifier (MEZ-8201, Nihon-Koden, Tokyo, Japan), digi-

tised, and recorded on a computer (SD-512, EPSON, Japan). The field potential responses were averaged over five trials.

2.3. Drugs

6-Cyano-7-nitroquinoxaline-2,3-dione (CNQX; a non-N-methyl-D-aspartate (NMDA) glutamate receptor antagonist), DL-2-amino-5-phosphonopentanoic acid (APV; an NMDA receptor antagonist), 8-cyclopentyl-1,3-dimethylxanthine (8-CPT; an adenosine A_1 receptor antagonist) and 2-chloro-N^6-cyclopentyladenosine (CCPA; an adenosine A_1 receptor agonist) were purchased from Sigma-Aldrich (Tokyo, Japan). 2-Carboxy-4-isopropyl-3-pyrrolidineacetic acid (DHK; a glial glutamate transporter antagonist) was purchased from Tocris Cookson (Bristol, UK). ω-AgaIVA and ω-CgTxGVIA were synthesized as described previously (Kim et al., 1994, 1995).

3. Results

3.1. Tonic inhibition of glutamate release at CA3–CA1 synapses by adenosine A_1 receptors

We have previously shown that glial glutamate transporter activity can be measured in the CA1 region of the hippocampus using an optical imaging technique (Kojima et al., 1999, Kawamura et al., 2004). Briefly, in normal artificial cerebrospinal fluid, the synaptically induced signals recorded from slices stained with the voltage-sensitive dye, RH155, consist of several components, including those due to presynaptic fibre volley, EPSPs and action potentials (Fig. 1A and B). In the presence of ionotropic glutamate receptor blockers, the signals due to EPSPs and action potentials disappear, leaving a slowly depolarising response that can be blocked by glutamate transporter blockers, such as DHK (Fig. 1B), and which is due to the depolarisation of astrocytes caused by the electrogenic activity of the GLT-1 glutamate transporter, which is stimulated by release of glutamate from the synapses. We therefore refer to this signal as synaptically induced glial depolarisation. The amplitude of the synaptically induced glial depolarisation signal is monotonically related to the intensity of stimulation (Fig. 1C–E).

In the present study, we examined whether application of an adenosine A_1 receptor antagonist substantially enhanced the synaptically induced glial depolarisation signal. Fig. 1C and D shows the effect of 0.5 μM 8-CPT on the synaptically induced glial depolarisation and field potential at three different stimulus intensities. In Fig. 1C and E1, the area of the synaptically induced glial depolarisation signal (0–120 ms) evoked by 0.1 or 0.3 mA was increased by 99.8% ($n=5$) and 150% ($n=5$), respectively. When the effect of 0.5 μM 8-CPT on the slope of the fEPSP was tested on a separate set of slice preparations (Fig. 1D), the slope of the fEPSPs

evoked by 0.05, 0.1 and 0.3 mA was increased by 216% ($n=5$), 105% ($n=5$) and 75% ($n=5$), respectively (Fig. 1E2).

To confirm that the effect of 8-CPT was really due to inhibition of the adenosine A_1 receptor, we examined the effect of 8-CPT on the inhibition induced by an adenosine A_1 receptor agonist and on control transmission. Bath application of the specific adenosine A_1 receptor agonist, CCPA (0.5 μM), reduced both the amplitude of the synaptically induced glial depolarisation (Fig. 2A) and the slope of the fEPSP (Fig. 2B) to 60±9.2% ($n=6$) and 31±12% ($n=4$) of control levels, respectively. Using a combination of 0.5 μM 8-CPT and 0.5 μM CCPA, the amplitude of the synaptically induced glial depolarisation and the slope of fEPSP returned not to the basal level, but to a much higher level, the amplitude of the synaptically induced glial depolarisation reaching 226±32% ($n=6$) and the slope of the fEPSP 145±41% ($n=4$) of control levels (Fig. 2A and B). The values for the amplitude of the synaptically induced glial depolarisation and the slope of the fEPSP in the presence of 8-CPT alone were not significantly different (synaptically induced glial depolarisation $p=0.34$; fEPSP $p=0.21$ paired t-test) from those in the presence of both CCPA and 8-CPT (Fig. 2C1 and C2). Fig. 3 shows the dose dependency of the effect of 8-CPT on the amplitude of the synaptically induced glial depolarisation. The EC_{50} value was 0.9±1.1 μM.

The synaptically induced glial depolarisation signals showed a paired-pulse facilitation for a paired pulse with a 50-ms inter-pulse interval, as did the field EPSPs (Figs. 1C and 2A). Interestingly, in contrast to the paired-pulse ratio for the slope of fEPSP, the paired-pulse ratio for the synaptically induced glial depolarisation was not significantly affected by the presence of CCPA or of 8-CPT (Fig. 2D).

These results confirm those of a previous report (Wu and Saggau, 1994a), which showed that synaptic transmission at CA3–CA1 synapses is tonically inhibited by activation of adenosine A_1 receptors. We also tested whether transmission was tonically inhibited by metabotropic glutamate receptors, but found that metabotropic glutamate receptor antagonists, such as (RS)-α-Methyl-4-phosphonophenylglycine (MPPG), had no significant effect on the amplitude of the synaptically induced glial depolarisation (data not shown).

3.2. Adenosine A_1 receptors control glutamate release by inhibiting N-type voltage-gated Ca^{2+} channels

To examine which voltage-gated Ca^{2+} channels were responsible for transmitter release and to understand the mechanisms by which adenosine A_1 receptors inhibit synaptic transmission, we compared the effects of blockers of P/Q- and N-type voltage-gated Ca^{2+} channels on the amplitude of the synaptically induced glial depolarisation in the presence and absence of 8-CPT. To block adenosine A_1 receptor-mediated inhibition, 10 μM 8-CPT was applied to
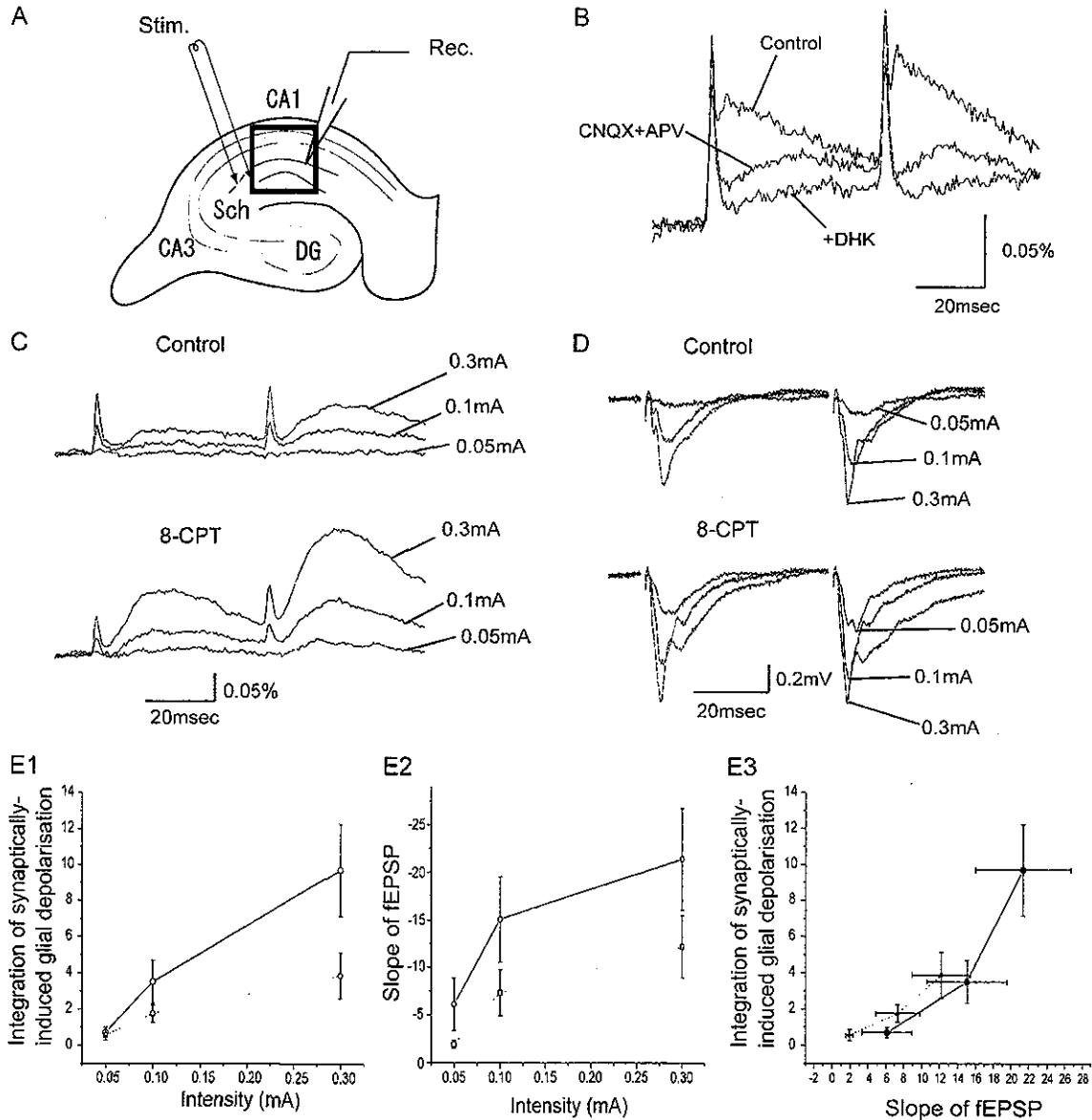
Fig. 1. Synaptically induced glial depolarisation monitored optically in the hippocampal CA1 area. (A) A slice was stained with a voltage-sensitive dye RH155. The slice was electrically stimulated by a bipolar electrode (Stim.) positioned in the stratum radiatum. An extracellular recording electrode (Rec.) was placed in the stratum radiatum to record the fEPSP. The changes in absorption were measured from the area indicated by a rectangle. (B) Sample traces of the change in absorption in response to a pair of stimuli recorded from the stratum radiatum. In control artificial cerebrospinal fluid, the response consists of three main components: a very fast spike-like component due to activity of presynaptic fiber volley, a fast component, and a slow component. Blockage of ionotropic glutamate receptors by applying CNQX (10 µM) and APV (50 µM) abolished the fast responses, leaving slow depolarising responses. Bath application of DHK (1 mM), a selective GLT-1 glutamate transporter antagonist, suppressed the synaptically induced glial depolarisation. (C, D) Synaptically induced glial depolarisation and fEPSP evoked by stimulus at various intensities (0.05–0.3 mA) in control conditions (top) and in the presence of 8-CPT (0.5 µM), a specific adenosine A₁ receptor blocker (bottom). (E1, E2) Dependence of the initial slope of the fEPSP (*n*=6) and the amplitude of the synaptically induced glial depolarisation (*n*=6) on stimulus intensity in control conditions (dashed line) and in the presence of 0.5 µM 8-CPT. (E3) The relationship between the fEPSP (*n*=6) and the synaptically induced glial depolarisation (*n*=6) at different stimulus intensities in control conditions (dashed line) and in the presence of 0.5 µM 8-CPT.

the bathing medium, then synaptically induced glial depolarisation was elicited by applying five repetitive stimuli at 10 ms intervals in order to increase the signal to noise ratio, a stimulation pattern which itself does not cause a change in the amplitude of the synaptically induced glial depolarisation (Kawamura et al., 2004). ω-AgaIVA was used to block P/Q-type channels and ω-CgTxGVIA to block N-

type channels; on the basis of the results of Wu and Saggau (1994b), to obtain a maximal effect, both blockers were applied at a concentration of 1 µM for 20 min before testing for suppression of synaptically induced glial depolarisation in the presence of the voltage-gated Ca^{2+} channel blockers.

Fig. 4 shows representative responses (Fig. 4A) and the summarised results (Fig. 4B) of the effects of Ca^{2+} channel
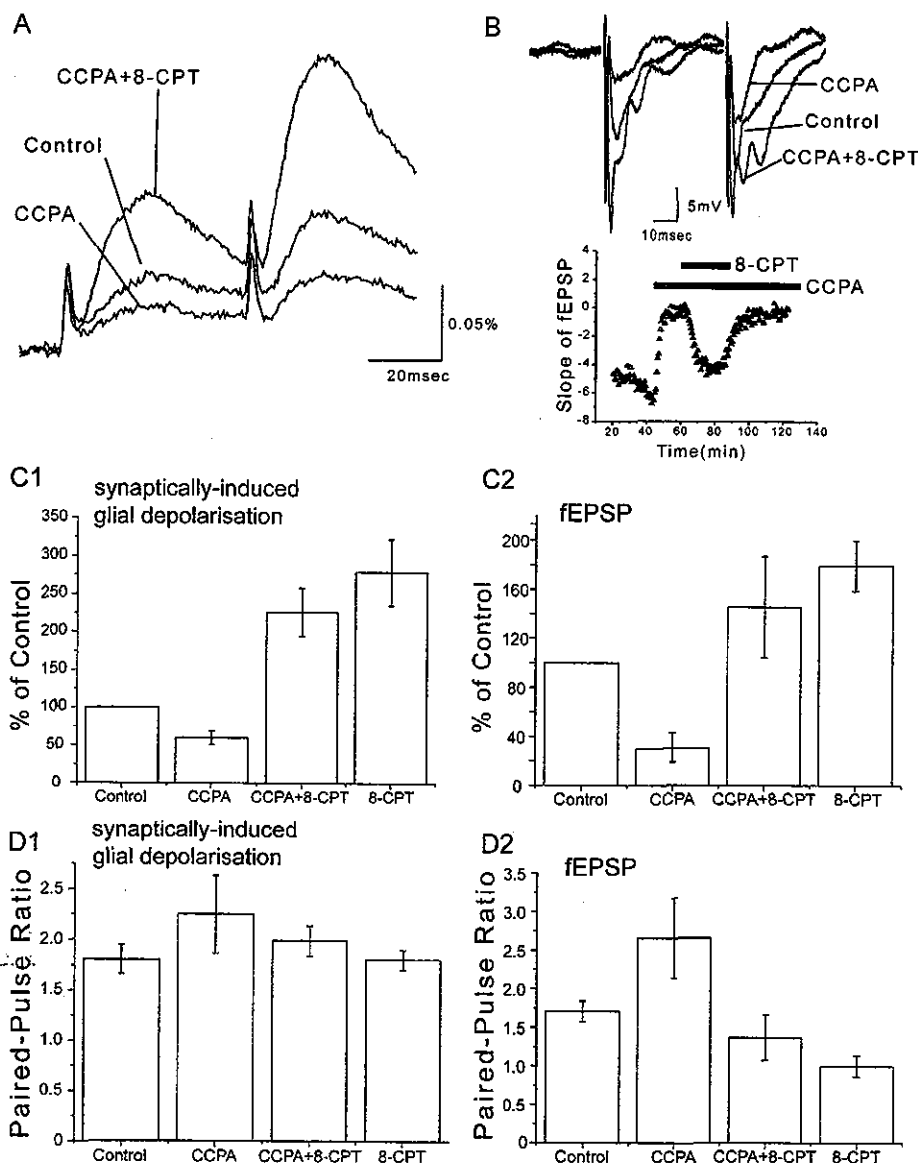
Fig. 2. Tonic inhibition of glutamate release by adenosine A_1 receptors. (A) Typical experiment showing the effects of application of CCPA (0.5 μM) and co-application of CCPA and 8-CPT (both 0.5 μM) on the synaptically induced glial depolarisation. CNQX(10 μM) and APV(50 μM) were present in the bath in all experiments. (B) Effects of application of CCPA (0.5 μM) and co-application of CCPA and 8-CPT (both 0.5 μM) on the fEPSP. Top: A typical experiment showing the field EPSPs. Bottom: Time-course of changes in the initial slope of the fEPSP during application of CCPA and co-application of CCPA and 8-CPT. Pooled data for the effects of CCPA alone and CCPA plus 8-CPT on the synaptically induced glial depolarisation (C1, n=4) and the fEPSP (C2, n=4). The signals were normalised to those before application of CCPA or 8-CPT. Effects of CCPA and co-application of CCPA and 8-CPT on the paired-pulse ratio of the synaptically induced glial depolarisation (D1) and the fEPSP (D2). Each column and bar indicates the mean and S.E.M.

blockers in the absence of 8-CPT. Both Ca^{2+} channel blockers suppressed the amplitude of the synaptically induced glial depolarisation without affecting the time-course of the effect. To estimate the relative contribution of different types of Ca^{2+} channels to transmitter release, the degree of suppression caused by a blocker of a specific Ca^{2+} channel type should be normalised to that caused by a potent non-specific Ca^{2+} channel blocker. In the presence of DHK, synaptically induced glial depolarisation was suppressed to such an extent that the addition of 300 μM Cd^{2+} to the bathing medium did not suppress the signal further (data not shown). To normalise the amplitude of the

synaptically induced glial depolarisation, we therefore subtracted the amplitude of the signal obtained in the presence of DHK from that obtained in its absence.

When the adenosine A_1 receptor was not blocked, application of ω-AgaIVA (1 μM) alone, ω-CgTxGVIA (1 μM) alone or co-application of ω-AgaIVA and ω-CgTxGVIA reduced the synaptically induced glial depolarisation to 44.4±6.5% (n=10), 67.4±7.3% (n=10) or 30.3±3.6% (n=10) of control levels, respectively (Fig. 4B). In contrast, in the presence of 8-CPT (10 μM), the corresponding values were 47.9±5.9% (n=6), 32.0±5.7% (n=4) or 22.7±7.7% (n=5) of control levels (Fig. 5B).
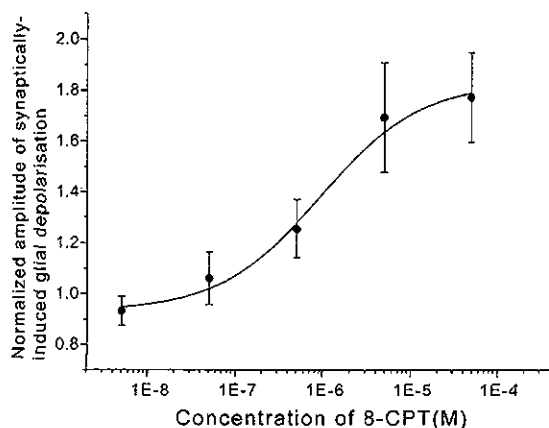
Fig. 3. Dose dependency of the effects of 8-CPT on the amplitude of the synaptically induced glial depolarisation. The amplitude of the synaptically induced glial depolarisation in the presence of 8-CPT was normalised to the value before applying 8-CPT. The bars show the S.E.M. ($n=6$). Data points were fitted to a sigmoidal curve ($Y=[-0.9/\{1+(x/EC^{50})^{0.8}\}+1.8]$) using the χ^2 method. The EC_{50} value was 0.9 ± 1.1 μM.

These results showed that, in the presence of adenosine A_1 receptor-mediated suppression, the contribution of the P/Q-type channel was greater than that of the N-type channel, but, when adenosine A_1 receptor-mediated suppression was

removed, the contribution of the N-type Ca^{2+} channel was greater than that of the P/Q-type channel.

4. Discussion

In this study, we monitored glutamate transmitter release by optically recording glial glutamate transporter activity, and found that the contribution of N-type voltage-gated Ca^{2+} channels to glutamate release was greater than that of P/Q-type voltage-gated Ca^{2+} channels when adenosine A_1 receptors were inhibited. This indicates that glutamate release at hippocampal CA3–CA1 synapse is tonically suppressed by activation of adenosine A_1 receptors and that the suppression is mainly due to inhibition of N-type voltage-gated Ca^{2+} channel.

The method we used in this study to measure glutamate release involved the monitoring of glutamate transporter activity in glial cells. We have shown in a previous report (Kojima et al., 1999) that the signal is due to glial transport on the basis that the signal can be recorded in a preparation in which postsynaptic cells are absent and that the signal was almost absent in slice preparations made from GLT-1 knock out mice. Still we cannot rule out the possibility that a
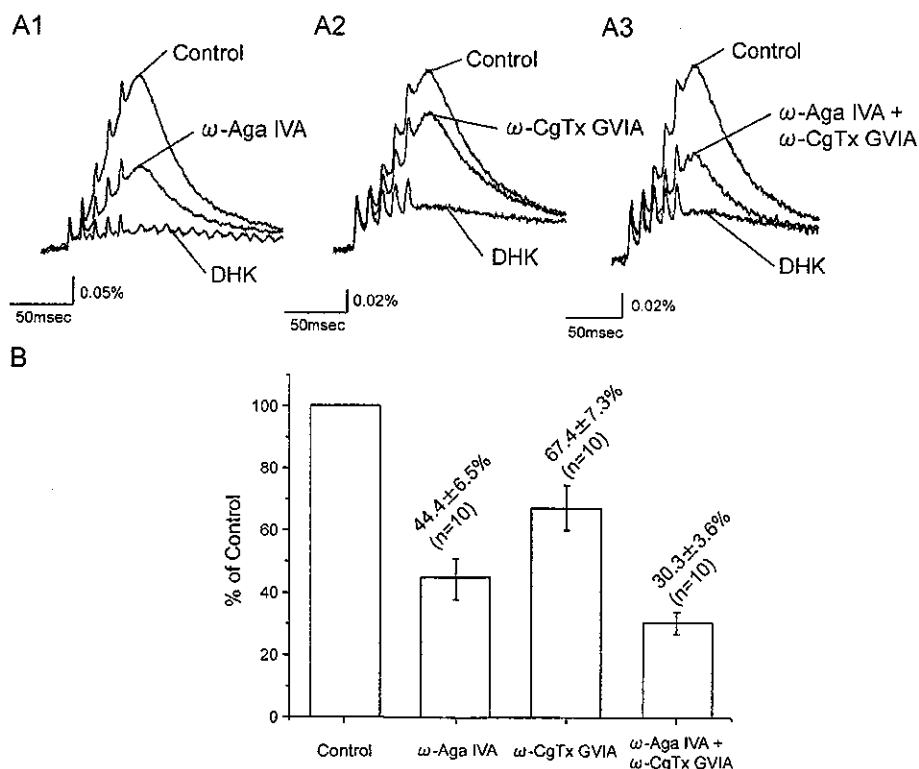

Fig. 4. Effects of Ca^{2+} channel blockers on the amplitude of the synaptically induced glial depolarisation in the absence of an adenosine A_1 receptor blocker. (A) The synaptically induced glial depolarisation was measured in normal artificial cerebrospinal fluid, and the blockers for the P/Q-type channel, ω-AgaIVA (1 μM, A1), and/or the N-type channel, ω-CgTxGVIA (1 μM, A2) were applied. Responses were evoked by delivering 5 stimuli with a 10-ms interval to Schaffer collaterals. The effect of application of ω-CgTxGVIA was smaller than that of ω-AgaIVA. Application of DHK (1 mM) suppresses the component due to glutamate uptake, leaving a component which is not related to glutamate release. CNQX (10 μM) and APV (50 μM) were present in the bath in all experiments. (B) Statistical comparison of the effects of Ca^{2+} channel blockers on the synaptically induced glial depolarisation in the absence of 8-CPT (10 μM). After subtracting the DHK-insensitive component, the signal was integrated over the first 200 ms and normalised to the value in control conditions. Each column and bar indicates the mean and S.E.M.
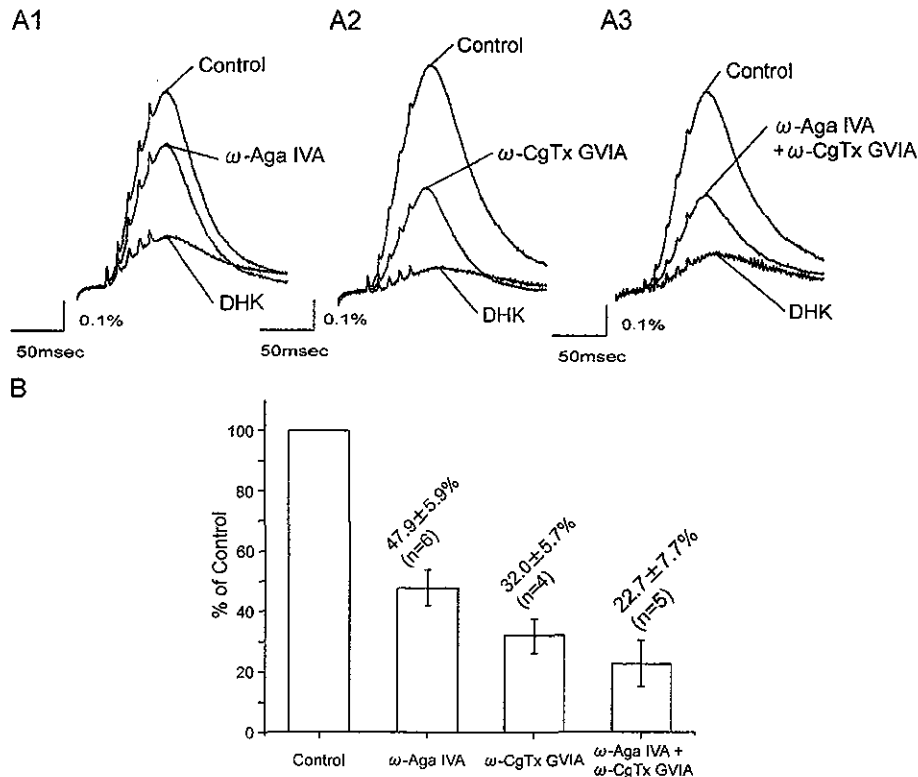
Fig. 5. Effects of Ca^{2+} channel blockers on the amplitude of the synaptically induced glial depolarisation in the presence of an adenosine A_1 receptor blocker. (A) The synaptically induced glial depolarisation was measured in the presence of 8-CPT (10μM), and the blockers for the P/Q-type channel, ω-AgaIVA (1 μM, A1), and/or the N-type channel, ω-CgTxGVIA (1 μM, A2) were applied. Responses were evoked by delivering five stimuli with a 10 ms interval to Schaffer collaterals. The effect of application of ω-CgTxGVIA was greater than that of ω-AgaIVA. Application of DHK (1 mM) suppresses the component due to glutamate uptake, leaving a component which is not related to glutamate release. CNQX(10 μM) and APV(50 μM) were present in the bath in all experiments. (B) Statistical comparison of the effects of Ca^{2+} channel blockers on the synaptically induced glial depolarisation in the presence of 8-CPT (10 μM). After subtracting the DHK-insensitive component, the signal was integrated over the first 200 ms and normalised to the value in control conditions. Each column and bar indicates the mean and S.E.M.

part of the synaptically induced depolarizing signal in the presence of glutamate receptor antagonists could be due to activities of neuronal glutamate transporters because the voltage-sensitive dye we used in this study preferentially stains glial cells but stains neuronal cells as well (Momose-Sato et al., 1999). If it was the case, however, it would not confound our results, because, either way we can monitor amount of glutamate release by measuring the signal that we refer to as synaptically induced glial depolarisation.

There is a possibility that the applied adenosine A_1 receptor agonist and/or antagonist acted on the glial glutamate transporter, rather than on transmitter release. However, application of the adenosine A_1 receptor blocker also facilitated the fEPSPs, implying that the blocker acted on release, not on uptake. To support presynaptic site of drug actions, an immunohistochemical study by Ochiishi et al. (1999) reported that adenosine A_1 receptor immunoreactivity was not detected on glial cells. In addition, it has been reported that glial transporters can be regulated by activation of adenosine A_2 receptors, but not adenosine A_1 receptors (Nishizaki et al., 2002). Thus, it is unlikely that the adenosine A_1 receptor agonist and/or antagonist acted on glial glutamate transporters.

Immunohistochemical studies reported that not only presynaptic but also post synaptic reactivities of adenosine A_1 receptors were detected (Ochiishi et al., 1999, Rebola et al., 2003), and that adenosine A_1 receptors co-localize with postsynaptic NMDA glutamate receptors and N- or P/Q-type voltage-gated Ca^{2+} channels (Rebola et al., 2003). Therefore adenosine A_1 receptor agonist and/or antagonist might have acted on postsynaptic sites. In our experimental condition, however, responses of postsynaptic neurons were blocked by antagonists against ionotropic glutamate receptors. Therefore, signals due to activities of postsynaptic membranes or due to uptake of glutamate from the recurrent terminals of post synaptic neurons were unlikely to be involved in synaptically induced glial depolarisation signal in this study.

It has been shown in previous reports that activation of presynaptic metabotropic glutamate receptors would suppress glutamate release from presynaptic terminals (Cartmell and Schoepp, 2000). To test this possibility, we tested the effects of agonists and antagonists for mGluRs on synaptically induced glial depolarisation signals in normal conditions in which the adenosine A_1 receptor agonist was absent. We found that mGluR agonists suppressed synap-

tically induced glial depolarisation significantly, whereas the antagonists did not significantly enhance synaptically induced glial depolarisation. Although N-type voltage-gated Ca^{2+} channel are the most common voltage-gated Ca^{2+} channels shown to be inhibited by mGluR agonists in literatures (Anwyl, 1999), it is possible that presynaptic mGluRs be more effectively activated in the presence of adenosine A_1 receptor antagonist and the activated mGluRs target P/Q voltage-gated Ca^{2+} channels. We have not tested the effects of mGluR agonists/antagonists in the presence of adenosine A_1 receptor antagonists. Still, we should be able to claim N-type voltage-gated Ca^{2+} channel as the main regulator in normal conditions.

Both in the presence and absence of 8-CPT, the degree of blockade after co-application of ω-AgaIVA and ω-CgTxGVIA was less than the sum of the blockades produced by ω-AgaIVA alone or ω-CgTxGVIA alone. This non-linearity is not surprising, since it has been shown by Reuter (Reuter, 1995) that ω-AgaIVA-sensitive voltage-gated Ca^{2+} channels and ω-CgTxGVIA-sensitive voltage-gated Ca^{2+} channels coexist in more than half of the synaptic terminals of hippocampal cell cultures, and, since the amplitude of the postsynaptic response is likely to be related to the power of the presynaptic Ca^{2+} current (Augustine et al., 1985), the non-linearity may be due to the power relationship between the presynaptic Ca^{2+} current and transmitter release at those terminals in which N- and P/Q-type voltage-gated Ca^{2+} channels coexist. If the tonic suppression of glutamate release mediated by adenosine A_1 receptors is mainly due to inhibition of voltage-gated Ca^{2+} channels, we should be able to estimate the degree of tonic inhibition of N- and P/Q-type voltage-gated Ca^{2+} channels by activation of adenosine A_1 receptors at CA3–CA1 synapses and also the relative contributions of these channels in the absence of inhibition. We assumed that the relationship between the amplitude of the synaptically
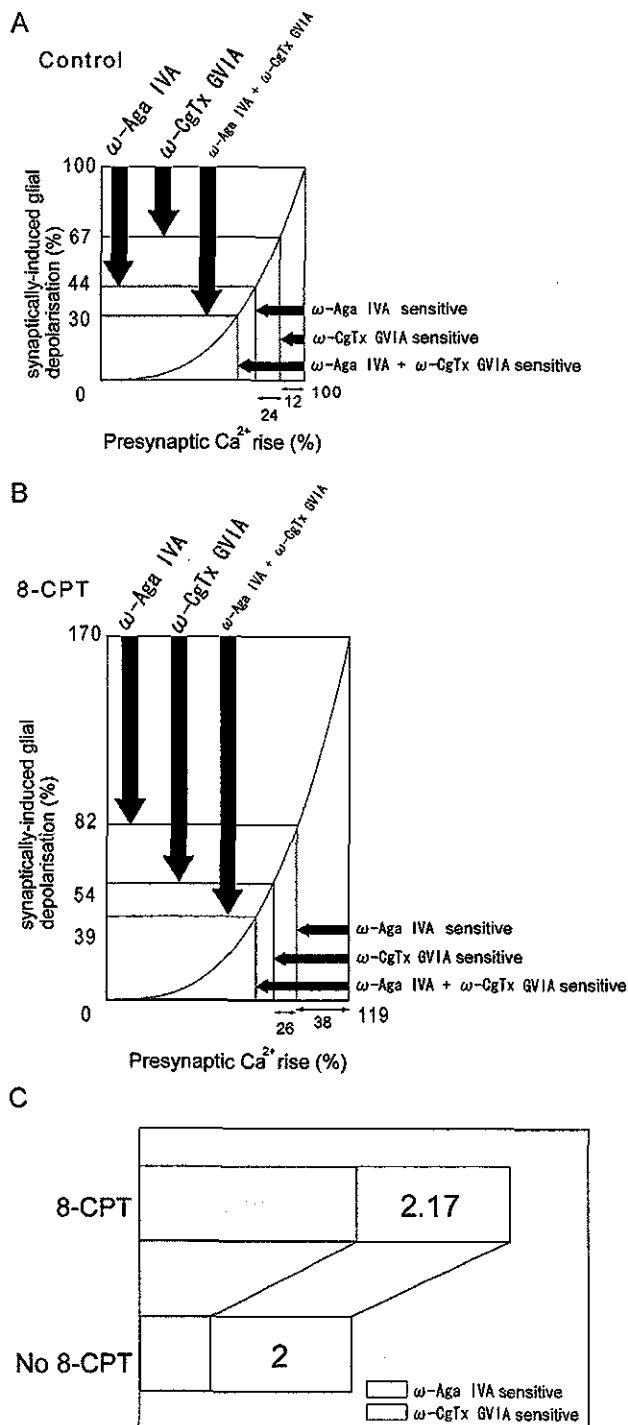

Fig. 6. An analysis of the contribution of voltage-gated Ca^{2+} channels to glutamate release. (A) The relationship between the synaptically induced glial depolarisation and the calculated presynaptic Ca^{2+} influx in the absence of an adenosine A_1 receptor blocker. In this calculation, the amplitude of the synaptically induced glial depolarisation was assumed to be proportional to the third power of the change in the $[Ca^{2+}]_{pre}$; synaptically induced glial depolarisation=constant×$(\Delta[Ca^{2+}]_{pre})^3$. The ordinate shows the relative amplitude of synaptically induced glial depolarisation normalized to the value in the control condition in which 8-CPT was absent. The vertical arrows show the extent of the suppression by blockers for voltage-gated Ca^{2+} channels. The abscissa shows the relative change in calculated presynaptic Ca^{2+} concentration normalized to the value in the control condition. The horizontal arrows show the extent of suppression. (B) The relationship between the synaptically induced glial depolarisation and the calculated presynaptic Ca^{2+} influx in the presence 8-CPT, an adenosine A_1 receptor blocker. The ordinate and the abscissa are normalized to the value obtained in the control condition in which 8-CPT was absent. (C) Comparison of the calculated contribution of voltage-gated Ca^{2+} channels to the change in the $[Ca^{2+}]_{pre}$. The values are normalised to the contribution of the ω-CgTxGVIA-sensitive component in the absence of adenosine A_1 receptor-mediated inhibition.

induced glial depolarisation and the Ca^{2+} rise due to entry through voltage-gated Ca^{2+} channels to be as follows.

Amplitude of the synaptically induced glial depolarisation

$$= constant \times \left(\Delta\left[Ca^{2+}\right]_{pre} \right)^m$$

Wu and Saggau (1994b) obtained a value of $m \approx 3.5$ by analysing their Ca^{2+} imaging data recorded from presynaptic terminals at CA3–CA1 synapses, simultaneously per-

A Control

B 8-CPT

C

Presynaptic Ca^{2+} rise (%)

ω-Aga IVA sensitive
ω-CgTx GVIA sensitive
ω-Aga IVA + ω-CgTx GVIA sensitive

8-CPT   2.17

No 8-CPT   2

ω-Aga IVA sensitive
ω-CgTx GVIA sensitive

formed with field EPSP measurements. Reid et al. (1998) estimated m=3.1 or 3.3 at hippocampal autapses. Reid et al. (1998) showed that the values for N- and P/Q-types were not significantly different. Applying this formula, we calculated the relative contribution of different voltage-gated Ca^{2+} channels to the Ca^{2+} rise, based on the effects of the different channel blockers on the synaptically induced glial depolarisation in the absence and in the presence of 8-CPT, the adenosine A_1 receptor blocker. In the absence of 8-CPT, the amplitude of synaptically induced glial depolarisation was reduced by ω-CgTxGVIA alone and ω-AgaIVA alone to 67.4±7.3% and 44.4±6.5% of the control respectively. For m=3, these values correspond to 12% and 24% blockade of the total Ca^{2+} rise (Fig. 6A). In the presence of 10 μM 8-CPT, the amplitude of the synaptically induced glial depolarisation increased to 170% (Fig. 3), corresponding to an increase in the Ca^{2+} rise of 119%. In this condition, the amplitude of synaptically induced glial depolarisation by ω-CgTxGVIA alone and ω-AgaIVA alone was 32.0±5.7% and 47.9±5.9% of control respectively, corresponding to 38% and 26% blockade of the total Ca^{2+} rise in the control conditions with no 8-CPT (Fig. 6B). Thus, the relative contribution of N- and P/Q-type voltage-gated Ca^{2+} channels was 1:2 in the absence of 8-CPT and 3.08:2.17 in the presence of 8-CPT (Fig. 6C). A similar conclusion was reached when we assume m=2, 4 or 5. We can therefore conclude that the N-type voltage-gated Ca^{2+} channel is suppressed by tonic activation of adenosine A_1 receptors, whereas the P-type voltage-gated Ca^{2+} channel is not significantly affected.

Although it has been shown that N- and P/Q-type voltage-gated Ca^{2+} channels are responsible for transmitter release at many synapses in the central nervous systems, the distribution and the contribution of these voltage-gated Ca^{2+} channels seem to vary from synapses to synapses (Reid et al., 1997, 2003; Reuter, 1996). Scholz and Miller (1995) and Iwasaki et al. (2000) also have shown that the relative contribution of N-type versus P/Q-type changes during development. The results of our study suggest a possibility that the extent of adenosine A_1 receptor-mediated tonic inhibition can be one of the reasons for the heterogeneity of voltage-gated Ca^{2+} channels responsible for transmitter release.

The source of adenosine responsible for tonic regulation of synaptic transmission is largely unknown, and we did not make attempts to analyze the source of adenosine in our study. Two possible sources have been suggested: dephosphorylation of ATP released either from presynaptic terminals or glial cells (Newman, 2003; Cunha and Ribeiro, 2000; Dunwiddie and Masino, 2001; Yawo and Chuhma, 1993). Release of adenosine via passive or active transporters is also suggested (Dunwiddie and Masino, 2001). The basal extracellular level of adenosine is reported to be in the range of 25–250 nM. Since the affinity of adenosine A_1 receptors to adenosine is reported to be around 70 nM (Dunwiddie and Masino, 2001), the basal level of adenosine

is high enough to provide tonic activation of adenosine A_1 receptors.

Acknowledgements

References

Ambrosio, A.F., Malva, J.O., Carvalho, A.P., Carvalho, C.M., 1997. Inhibition of N-, P/Q- and other types of Ca^{2+} channels in rat hippocampal nerve terminals by the adenosine A1 receptor. Eur. J. Pharmacol. 340, 301–310.

Anwyl, R., 1999. Metabotropic glutamate receptors: electrophysiological properties and role in plasticity. Brain Res. Rev. 29, 83–120.

Augustine, G.J., Charlton, M.P., Smith, S.J., 1985. Ca^{2+} entry into voltage-clamped presynaptic terminals of squid. J. Physiol. 367, 143–162.

Cartmell, J., Schoepp, D.D., 2000. Regulation of neurotransmitter release by metabotropic glutamate receptors. J. Neurochem. 75, 889–907.

Cunha, R.A., Ribeiro, J.A., 2000. ATP as a presynaptic modulator. Life Sci. 68, 119–137.

Dunwiddie, T.V., Masino, S.A., 2001. The role and regulation of adenosine in the central nervous system. Annu. Rev. Neurosci. 24, 31–55.

Iwasaki, S., Momiyama, A., Uchitel, O.D., Takahashi, T., 2000. Developmental changes in Ca^{2+} channel types mediating central synaptic transmission. J. Neurosci. 20, 59–65.

Kawamura, Y., Manita, S., Nakamura, T., Inoue, M., Kudo, Y., Miyakawa, H., 2004. Glutamate release increases during mossy-CA3 LTP but not during Schaffer-CA1 LTP. Eur. J. Neurosci. 19, 1591–1600.

Kim, J.I., Takahashi, M., Ogura, A., Kohno, T., Kudo, Y., Sato, K., 1994. Hydroxyl group of Tyr13 is essential for the activity of omega-conotoxin GVIA, a peptide toxin for N-type Ca^{2+} channel. J. Biol. Chem. 269, 23876–23878.

Kim, J.I., Konishi, S., Iwai, H., Kohno, T., Gouda, H., Shimada, I., Sato, K., Arata, Y., 1995. Three-dimensional solution structure of the Ca^{2+} channel antagonist omega-agatoxin IVA: consensus molecular folding of Ca^{2+} channel blockers. J. Mol. Biol. 250, 659–671.

Kojima, S., Nakamura, T., Nidaira, T., Nakamura, K., Ooashi, N., Ito, E., Watase, K., Tanaka, K., Wada, K., Kudo, Y., Miyakawa, H., 1999. Optical detection of synaptically induced glutamate transport in hippocampal slices. J. Neurosci. 19, 2580–2588.

Luebke, J.I., Dunlap, K., Turner, T.J., 1993. Multiple Ca^{2+} channel types control glutamatergic synaptic transmission in the hippocampus. Neuron 11, 895–902.

Misgeld, U., Bijak, M., Jarolimek, W., 1995. A physiological role for $GABA_B$ receptors and the effects of baclofen in the mammalian central nervous system. Prog. Neurobiol. 46, 423–462.

Mogul, D.J., Adams, M.E., Fox, A.P., 1993. Differential activation of adenosine receptors decreases N-type but potentiates P-type Ca^{2+} current in hippocampal CA3 neurons. Neuron 10, 327–334.

Momose-Sato, Y., Sato, K., Arai, Y., Yazawa, I., Mochida, H., Kamino, K., 1999. Evaluation of voltage-sensitive dyes for long-term recording of neural activity in the hippocampus. J. Membr. Biol. 172, 145–157.

Newman, E.A., 2003. New roles for astrocytes: regulation of synaptic transmission. Trends Neurosci. 26, 536–542.

Nishizaki, T., Nagai, K., Nomura, T., Tada, H., Kanno, T., Tozaki, H., Li, X.X., Kondoh, T., Kodama, N., Takahashi, E., Sakai, N., Tanaka, K., Saito, N., 2002. A new neuromodulatory pathway with a glial contribution mediated via A(2a) adenosine receptors. Glia 39, 133–147.

Ochiishi, T., Saitoh, Y., Yukawa, A., Saji, M., Ren, Y., Shirao, T., Miyamoto, H., Nakata, H., Sekino, Y., 1999. High level of adenosine A_1 receptor-like immunoreactivity in the CA2/CA3a region of the adult rat hippocampus. Neuroscience 93, 955–967.

Rebola, N., Pinheiro, P.C., Oliveira, C.R., Malva, J.O., Cunha, R.A., 2003. Subcellular localization of adenosine A_1 receptors in nerve terminals and synapses of the rat hippocampus. Brain Res. 987, 49–58.

Reid, C.A., Clements, J.D., Bekkers, J.M., 1997. Nonuniform distribution of Ca^{2+} channel subtypes on presynaptic terminals of excitatory synapses in hippocampal cultures. J. Neurosci. 17, 2738–2745.

Reid, C.A., Bekkers, J.M., Clements, J.D., 1998. N- and P/Q type Ca^{2+} channels mediate transmitter release with a similar cooperativity at rat hippocampal autapses. J. Neurosci. 18, 2849–2855.

Reid, C.A., Bekkers, J.M., Clements, J.D., 2003. Presynaptic Ca^{2+} channels: a functional patchwork. Trends Neurosci. 26, 683–687.

Reuter, H., 1995. Measurements of exocytosis from single presynaptic nerve terminals reveal heterogeneous inhibition by Ca^{2+}-channel blockers. Neuron 14, 773–779.

Reuter, H., 1996. Diversity and function of presynaptic Ca^{2+} channels in the brain. Curr. Opin. Neurobiol. 6, 331–337.

Schlicker, E., Kathmann, M., 2001. Modulation of transmitter release via presynaptic cannabinoid receptors. Trends Pharmacol. Sci. 22, 565–572.

Scholz, K.P., Miller, R.J., 1995. Developmental changes in presynaptic Ca^{2+} channels coupled to glutamate release in cultured rat hippocampal neurons. J. Neurosci. 15, 4612–4617.

Takahashi, T., Momiyama, A., 1993. Different types of Ca^{2+} channels mediate central synaptic transmission. Nature 366, 156–158.

Vizi, E.S., 2000. Role of high-affinity receptors and membrane transporters in nonsynaptic communication and drug action in the central nervous system. Pharmacol. Rev., 63–89.

Wheeler, D.B., Randall, A., Tsien, R.W., 1994. Roles of N-type and Q-type Ca^{2+} channels in supporting hippocampal synaptic transmission. Science 264, 107–111.

Wu, L.G., Saggau, P., 1994. Adenosine inhibits evoked synaptic transmission primarily by reducing presynaptic Ca^{2+} influx in area CA1 of hippocampus. Neuron 12, 1139–1148.

Wu, L.G., Saggau, P., 1994. Pharmacological identification of two types of presynaptic voltage-dependent Ca^{2+} channels at CA3–CA1 synapses of the hippocampus. J. Neurosci. 14, 5613–5622.

Wu, L.G., Saggau, P., 1997. Presynaptic inhibition of elicited neurotransmitter release. Trends Neurosci. 20, 204–212.

Yawo, H., Chuhma, N., 1993. Preferential inhibition of ω-conotoxin-sensitive presynaptic Ca^{2+} channels by adenosine autoreceptors. Nature 365, 256–258.

M. Nakamura*
Y. Ishida
T. Kohno
K. Sato
Y. Oba
H. Nakamura†

Effects of modification at the fifth residue of μ-conotoxin GIIIA with bulky tags on the electrically stimulated contraction of the rat diaphragm

Authors' affiliations:

M. Nakamura, Y. Oba and H. Nakamura,
Graduate School of Bioagricultural Sciences,
Nagoya University, Chikusa-ku, Nagoya,
464-8601, Japan

Y. Ishida, T. Kohno and K. Sato, Mitsubishi
Kagaku Institute of Life Sciences, Machida,
Tokyo, 194-8511, Japan

K. Sato, Fukuoka Women's University, Higashi-
ku, Fukuoka, 813-8529, Japan

Correspondence to:

M. Nakamura
Department of Applied Physics and Chemistry
The University of Electro-Communications
Chofu
Tokyo
182-8585
Japan
Tel.: 81-424-86-1966
Fax: 81-424-86-1966
E-mail: mnak@pc.uec.ac.jp

*Present address: Department of Applied Physics
and Chemistry, The University of Electro-
Communications, Chofu, Tokyo, 182-8585, Japan.
†Deceased November 9, 2000.

Abstract: μ-Conotoxin GIIIA, a peptide toxin from the cone snail,
blocks muscle-type sodium channels. Thr-5 of μ-conotoxin GIIIA,
located on the opposite side of the active site in the globular
molecule, was replaced by Cys to which the bulky tags were
attached. The tagged μ-conotoxin GIIIA derivatives, except for the
phospholipid-tagged one, exerted the biological activity with a
potency slightly weaker than natural μ-conotoxin GIIIA. When the
biotinylated tags of various lengths were added, the presence of
avidin suppressed the action of the biotinylated toxins of <4 nm,
but not with 5 nm. The bulky biotinylated tags are useful as a
caliper to measure the depth of receptor sites in the channels.

Abbreviations: Biotin20, N'-[2-(N-Maleimido)ethyl]-N-piperazinyl
D-biotinamide; Biotin30, 6-{N'-[2-(N-maleimido)ethyl]-
N-piperazinylamide}hexyl D-biotinamide; BM(PEO)$_4$, 1,11-bis-
maleimidotetraethyleneglycol; Fmoc, 9-fluorenylmethyloxy
carbonyl; GIIIA, μ-conotoxin GIIIA; lipid, N-[(4-
maleimidylmethyl)cyclohexyl-1-carbonyl]-1,2-dihexadecanoyl-
n-glycero-3-phosphoethanolamine; MALDI-TOF-MS, matrix-
assisted laser desorption ionization time-of-flight mass
spectrometry; steroid, U-73122.

Introduction

Sodium channels are transmembrane proteins responsible
for the voltage-dependent increase in the sodium per-
meability that initiates action potentials [1]. The pore-
forming α-subunit of the sodium channels consists of four
homologous domains [2]. Receptor site I sodium channel
toxins such as tetrodotoxin, saxitoxin and μ-conotoxins

block the sodium flux by physically occluding this channel pore (3,4).

μ-Conotoxin GIIIA (GIIIA) is a 22-amino acid peptide toxin isolated from the cone snail *Conus geographus* (Fig. 1) (3,5–8). The three-dimensional structure of GIIIA determined by nuclear magnetic resonance (NMR) (9–11) reveals that this peptide toxin conforms to a discoidal core structure with three intramolecular disulfide bridges and three hydroxyprolines that impart extreme structural rigidity to its backbone. Using μ-conotoxin, the functional roles of numerous pore residues have been elucidated (12–16). The most critical toxin–channel interaction pair identified to date is between Arg-13 of GIIIA and Glu-758 in domain II of the sodium channels (the rat skeletal muscle isoform numbering) with interactions of which about half was electrostatic and half non-electrostatic (12). Furthermore, using μ-conotoxin, the clockwise arrangement of the four internal domains of the sodium channel was revealed (17,18).

Recently, we modified a single amino acid of GIIIA to obtain ligands that are useful for studying the structure–activity relationships of GIIIA (19,20). The Arg-13 modification of GIIIA suggested that both the chemical nature of the guanidium group and its precise position within the pore are important for the activity of GIIIA (20). In contrast, replacing Thr-5 with Ala did not affect the activity of GIIIA (11), as the peptide segment between Cys-4 and Cys-10 faces an opposite side from the active site. Thus, we replaced Thr-5 with Cys to create the toxin derivative [Cys⁵]GIIIA, whose free thiol group enables the addition of various chemical groups (19). The three-dimensional structure of [Cys⁵]GIIIA was confirmed by circular dichroism (CD) and NMR spectra, and the free SH position of [Cys⁵]GIIIA was confirmed by the mass spectrometric method (19). The addition of small tags only modestly affected the biological activity when compared with that of natural GIIIA (19). In this study, our objective is to show that by using bulky tags, the relatively extensive decoration

Figure 1. The structure of μ-conotoxin GIIIA (upper) and various tags introduced at the Thr-5 position (bottom). The numbers indicate the amino acid order from the N-terminal.
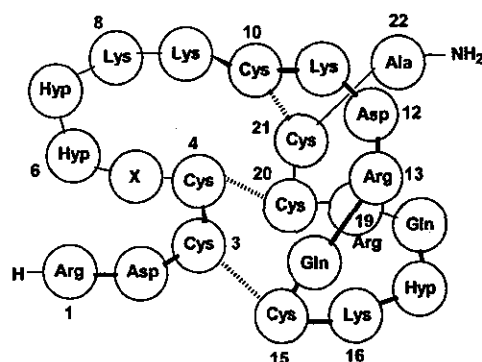
μ-conotoxin GIIIA :
X = Thr
Derivatives :
X = Cys, Lys(biotin), Cys(Tag)

Tag: